iScience

CellPress
OPEN ACCESS

Review

Shedding light on the energy applications of emerging 2D hybrid organic-inorganic halide perovskites

Neng Li,[1,2,5,*] Yufei Yang,[1] Zuhao Shi,[1] Zhigao Lan,[3,*] Arramel Arramel,[4] Peng Zhang,[5] Wee-Jun Ong,[6] Jizhou Jiang,[7,*] and Jianfeng Lu[1]

SUMMARY

Unique performance of the hybrid organic-inorganic halide perovskites (HOIPs) has attracted great attention because of their continuous exploration and breakthrough in a multitude of energy-related applications. However, the instability and lead-induced toxicity that arise in bulk perovskites are the two major challenges that impede their future commercialization process. To find a solution, a series of two-dimensional HOIPs (2D HOIPs) are investigated to prolong the device lifetime with highly efficient photoelectric conversion and energy storage. Herein, the recent advances of 2D HOIPs and their structural derivatives for the energy realms are summarized and discussed. The basic understanding of crystal structures, physicochemical properties, and growth mechanisms is presented. In addition, the current challenges and future directions to provide a roadmap for the development of next generation 2D HOIPs are prospected

INTRODUCTION

Since the advancement of industrialized society and the increasing demand for energy, the fossil fuel-based energy structures faced unprecedented challenges. Currently, more than 80% of the world's energy demand is mainly produced from the burning of fossil fuels, promoting massive flux of natural environmental threats such as global warming, air pollution, water pollution, and the depletion of natural resources, which are receiving urgent attention (Wang et al., 2015a). Concerted efforts have been made to minimize the effect of environmental pollution and to reduce the consumption of traditional energy (Ng et al., 2021; Ong et al., 2020a; Ong and Shak, 2020b; Peng et al., 2019; Zhang et al., 2020a). To name a few, solar energy is an ideal candidate for a clean energy source that is readily available, abundant in reserves, sustainable, easily-accessible, and environmentally-friendly. Therefore, the exploration of new materials has become a focal area in the context of energy research.

To meet the energy challenge, many researchers have studied how to enhance the conversion of solar energy, they have focused on the traditional perovskite oxide ABO_3, where "A" stands for rare earth or alkaline earth metal, and "B" represents a first-row transition metal. In similar fashion, the crystal structure of the halide perovskite material is similar to that of the general formula ABX_3, where A site is Cs or organic cation, the B site is a smaller cation (Pb, Sn, and Ge), and the "X" is a halide anion that bonds to the "A" and "B" cations. This material has attracted people's attention in the field of catalysis (Chen et al., 2020; Zejian et al., 2021). Ever since $CH_3NH_3PbI_3$ ($MAPbI_3$) was first applied to dye-sensitized solar cells by Miyasaka' group (Kojima et al., 2009), a great progress has been shown in the evolution of the power conversion efficiencies (PCE) of lead halide perovskite solar cells within a few years. The recorded PCE of $MAPbI_3$-based DSSC increased rapidly from 3.8% in 2009 to 22.1% in 2016 (Kojima et al., 2009; Chen et al., 2015; Jeon et al., 2014; Jeon et al., 2015; Lee et al., 2012; Liu et al., 2013; McMeekin et al., 2016; Saliba et al., 2016a; Saliba et al., 2016b; Shao et al., 2016; Shin et al., 2017; Yang et al., 2015; Zhou et al., 2014), which fascinates the development of photovoltaic industry. The results show that the excellent and distinctive photovoltaic characteristics of halide perovskites are the main reason for its rapid improvement, such as a favorable band gap, extremely high optical absorption coefficients, a strong defect tolerance, and shallow point defects, ultra-long photogenerated carrier lifetime, as well as the unprecedented long diffusion length compared to the other polycrystalline thin film solar cell materials. In addition, halide perovskites also have good application prospects in other energy fields (Kim et al., 2018, 2020a). For example, halide

[1]State Key Laboratory of Silicate Materials for Architecture, Wuhan University of Technology, Wuhan 430070, China

[2]Shenzhen Research Institute of Wuhan University of Technology, Shenzhen 518000, China

[3]Institute of New Materials & College of Physics and Telecommunications, Huanggang Normal University, Huangzhou 438000, China

[4]Department of Physics, National University of Singapore, 2 Science Drive 3, Singapore 117551, Singapore

[5]School of Materials Science and Engineering, Zhengzhou University, Zhengzhou 450001, China

[6]School of Energy and Chemical Engineering, Xiamen University Malaysia, Sepang Selangor Darul Ehsan 43900, Malaysia

[7]School of Environmental Ecology and Biological Engineering & School of Chemistry and Environmental Engineering, Key Laboratory of Green Chemical Engineering Process of Ministry of Education, Engineering Research Center of Phosphorus Resources Development and Utilization of Ministry of Education, Wuhan Institute of Technology, Wuhan 430205, Hubei, P. R. China

*Correspondence: lineng@whut.edu.cn (N.L.), 214129814@qq.com (Z.L.), 027wit@163.com (J.J.)

https://doi.org/10.1016/j.isci.2022.103753

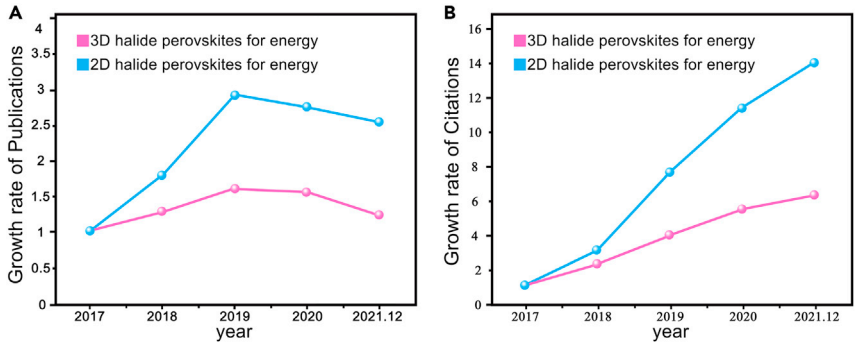

Figure 1. Research trends of halide perovskites for energy in the past five years

The growth rate (compared to the first year) of (A) publications and (B) citations of articles on "2D halide perovskites for energy", "3D halide perovskites for energy" in the last 5 years (the data is from the database Web of Science as of December 2021).

perovskite has current-voltage (I-V) hysteresis behavior, which makes it applicable to resistance switching memory (Choi et al., 2017; Kim et al., 2019a, 2020b).

However, the bulk (three-dimensional, 3D) halide perovskite still has two major problems, namely thermodynamics instability and lead toxicity, which are the main obstacles on the road to commercialization. Therefore, researchers are continuously trying to solve the fundamental problems that shrouding the limiting factors of bulk halide perovskites. The low-dimensionality of materials has become a choice for many researchers to explore material modification (Li et al., 2021; Xu et al., 2018a). Then, 2D organic-inorganic halide perovskites (2D HOIPs) nanomaterials have garnered great attention because of their unprecedented physical properties and their hold great promise compared to their bulk counterparts (Jiang et al., 2019). As shown in Figure 1, the number of citations has increased rapidly each year, and the growth rate of 2D perovskites is obviously higher than that of 3D perovskites, which shows that more and more researchers have discovered the research prospects of this material.

Unlike 3D halide perovskites, 2D HOIPs is able to incorporate bigger, less-volatile, and hydrophobic organic cations that promote the active materials with better thermal stability and chemical stability. To this end, we have summarized and compared the relevant properties of 2D and 3D halide perovskites in Table 1, using solar cells as an example. Moreover, 2D HOIPs feature the strong light-matter interaction, tunable thickness-dependent properties, structural relaxation, and photoluminescence shift. This structure can be considered as natural multiple quantum wells, where the insulating organic layers served as potential "barriers" and the semiconducting inorganic layers served as potential "wells" (Kataoka et al., 1993; Muljarov et al., 1995). In this configuration, the electronic confinement emerges in subnanometer layers that lead to the formation of stable excitons with exceptionally high binding energy. Moreover, the Bohr radius could expand beyond the limit of a single layer, because of not only dimensional confinement but also the dielectric properties modulated by the organic material. Consequently, the 2D HOIPs are useful in the field of electronic and optical devices, such as field-efiect transistors (FETs) (Kagan et al., 1999) and light-emitting diodes (LEDs) (Ishihara et al., 1989; Shang et al., 2019; Wang et al., 2016) for their unique optoelectronic performance. Studies have also shown that the photovoltaic performance of 2D HOIPs can be enhanced by adjusting non-covalent interactions (such as "CH$\cdots\pi$" interaction) (Yan et al., 2020).

In recent studies, researchers have studied the semiconductor physics of layered perovskites (Blancon et al., 2020; Mauck and Tisdale, 2019). Some researchers reviewed the properties, preparation, and application of low-dimensional perovskites. Although some researchers have reviewed 2D HOIPs applications in the direction of optoelectronic devices (Zhang et al., 2020b), a systematic review of the application of 2D HOIPs in energy has not yet appeared. At the same time, there is an increase in number of literatures everyday, which deserves another focused review. In this review, the progress of 2D HOIPs materials in recent years is summarized, including some 3D layered HOIPs materials, and in particular current advances in terms of their applications for photoelectric conversion, energy storage, photovoltaics, LEDs, batteries, supercapacitors, and thermoelectrics are reviewed. Meanwhile, the corresponding basic theoretical developments, which are beneficial to understand how 2D HOIP's excellent and unique photovoltaic

Table 1. Comparison of characteristics between 2D and 3D halide perovskites in solar cell

Perovskite	Dimension	Band gap	PCE(%)	V_{oc}(V)	Stability	Ref
$MAPbI_3$	3D	1.55	21.09	1.076	NA	(Chen et al., 2019a)
$MAPbI_3$	3D	1.55	14.8	1.04	NA	(Guo et al., 2017a)
$MAPbI_3$	3D	1.55	16.79	1.04	86% after 50 days in air	(Guo et al., 2019)
$MAPbICl_2$	3D	1.65	9.3	0.82	NA	(Mehdi et al., 2020)
$FAPbI_3$	3D	1.53	19.5	1.07	NA	(Jo et al., 2016)
α-$FAPbI_3$	3D	1.53	25.21	1.174	65% for reference cell and 90% for target cell after 1000 h in the dark at 25°C RH 20	(Jeong et al., 2021)
$BA_2MA_3Pb_4I_{13}$	quasi-2D	1.52–2.43	12.51	1.01	70% after 2250 h in RH 65 under light	(Tsai et al., 2016)
PEI_2PbI_4-$MAPbI_3$	quasi-2D	2.3	16.06	1.08	90% after 200 h in RH 50 under dark	(Yao et al., 2015)
$MAPbI_3$-PEA_2PbI_4	quasi-2D	NA	19.89	1.17	64% after 30 days in RH 20–30 under dark	(Bai et al., 2017)
$GA_2MA_4Pb_5I_{16}$	2D	NA	19.3	1.17	94% after more than 3000 h storage under ambient conditions	(Huang et al., 2021)
$FA_xPEA_{1-x}PbI_3$	2D	1.52	17.7	1.04	Stability measured at maximum power point up to 2 weeks	(Li et al., 2017)
$(BA)_2(MA)_{n-1}Pb_nI_{3n+1}$	2D	NA	19.56	1.11	96.5% after 100 h at 95°C under dark	(Lin et al., 2018)
$(PEI)_2(MA)_6Pb_7I_{22}$	2D	1.62	10.08	1.10	90% after 100 h under light	(Yao et al., 2016)
$(CA)_2(MA)_{n-1}Pb_nI_{3n+1}$	2D	1.63	9.03	0.88	NA	(Koh et al., 2016)

characteristics are produced, are also reviewed. As shown in Figure 2, we summarize an overview of outstanding developments in the field of 2D HOIPs(Kagan et al., 1999; Mitzi et al., 1994; Even et al., 2013; Smith et al., 2014; Dou et al., 2015; Ha et al., 2016; Stoumpos et al., 2017; Liu et al., 2017a; Mao et al., 2018; Shao et al., 2018; Zhang et al., 2019a; Lin et al., 2019). Finally, the perspectives and outlooks are involved in this review of the emerging 2D HOIPs materials, i.e., designing the highly anticipated lead-free perovskite to resolve the Pb toxicity, air-instability, and temperature-instability issues.

Rational design of 2D HOIPS

2D HOIPs structure

S.N. Ruddlesden and P. Popper first reported the crystal structure of 2D layered inorganic perovskites in 1957 (Ruddlesden and Popper, 1958). The periodical arrangements consist of 2D perovskite layers interleaved with cations and therefore named after these two pioneers as Ruddlesden-Popper (RP) perovskites. The 2D HOIPs materials are analogues of RP phase structure and represent the general formula of $L_2A_{n-1}B_nX_{3n+1}$. In the molecular formula, L stands for a large cation, A represents a regular cation such as Cs^+ or MA^+, B stands for a divalent metal cation such as Pb^{2+} or Sn^{2+}, and X is a halide. In this formula, n denotes the number of the octahedral stacking layers of metal halide sheets. The intergrowth of two L cation layers and n metal halide octahedral layers formed the 2D HOIPs structure. In this structure, apart from the van der Waals interaction between different units, the inorganic perovskite layers can be combined with organic perovskite layers by either ionic bonding or hydrogen bonding. Therefore, the 2D HOIPs structures are stabilized by different types of interactions compared to the bulk perovskite structure.

The basic units of 2D HOIPs and its morphological structure are shown in Figures 3A and 3B, respectively. The single-layer 2D HOIP is an ideal quantum well (QW) material. Typically, the "A" site is occupied by methylammonium (MA^+) ligands; the organic layers can be single or double layers depending on the ammonium compounds (Stoumpos et al., 2017). The RP phase perovskite is such a structure with a double-layered organic layer. The weak van der Waals interactions between the organic layers of this structure affect the structural stability of the perovskite. In contrast, the Dion-Jacobson (DJ) phase composed of single organic layer, and its organic cations and inorganic perovskite layers are connected by hydrogen bonds instead of weak van der Waals interactions between the organic layers, and thus exhibit better structural stability (Mao et al., 2018; Mao et al., 2019; Tremblay et al., 2019). We have provided common organic cations in 2D HOIPs in Table 2. In addition, the 2D halide perovskites can be obtained by reducing the thickness of the corresponding perovskite through delamination. The top and bottom surfaces are terminated by "A" cations instead of "L" cations (Shi et al., 2018).

Table 2. Common organic cations

Organic cation	Molecular structure	Organic cation	Molecular structure
MA	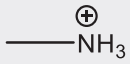	EA	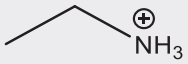
PA	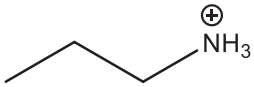	BA	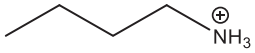
i-BA	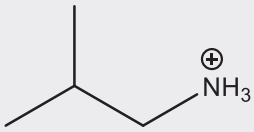	BYA	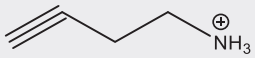
FA	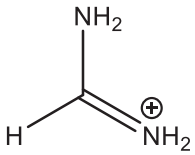	GA	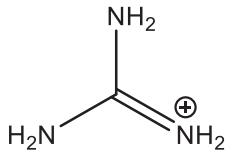
N-MPA	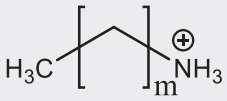	N-MEDA	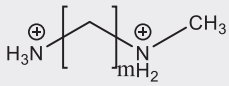
3AMP	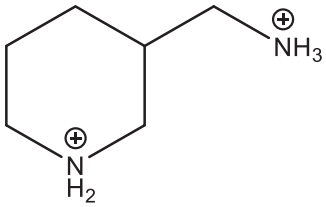	4AMP	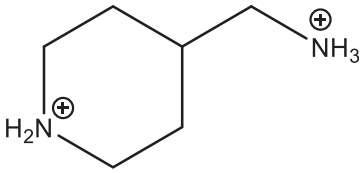
PEA	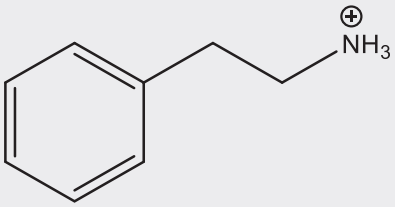	PMA	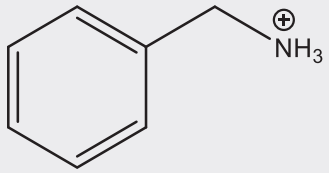
CEA	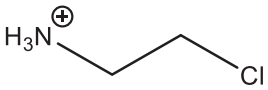	BEA	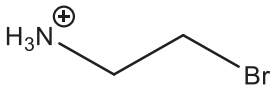

A property that is closely related to the crystal structure of 2D HOIPs is their electronic bandgaps. It is widely accepted that the flexibility of both crystal structure and electronic properties gives these 2D HOIPs great opportunities for diverse physicochemical properties such as crystal phase, bandgap energy, and effective mass of carriers. As such, a wide range of studies have been devoted to choosing different cations to achieve band gap regulation, and finding the most suitable cation for their required performance is also a major challenge for researchers. A summary of bandgap energy of typical 2D HOIPs is shown in Figure 3C. In addition, there are some other challenges in the application of 2D HOIP, such as stability, lead toxicity, and the possibility of large-scale production. Therefore, an extended overview will be introduced in the following synthesis and theoretical section.

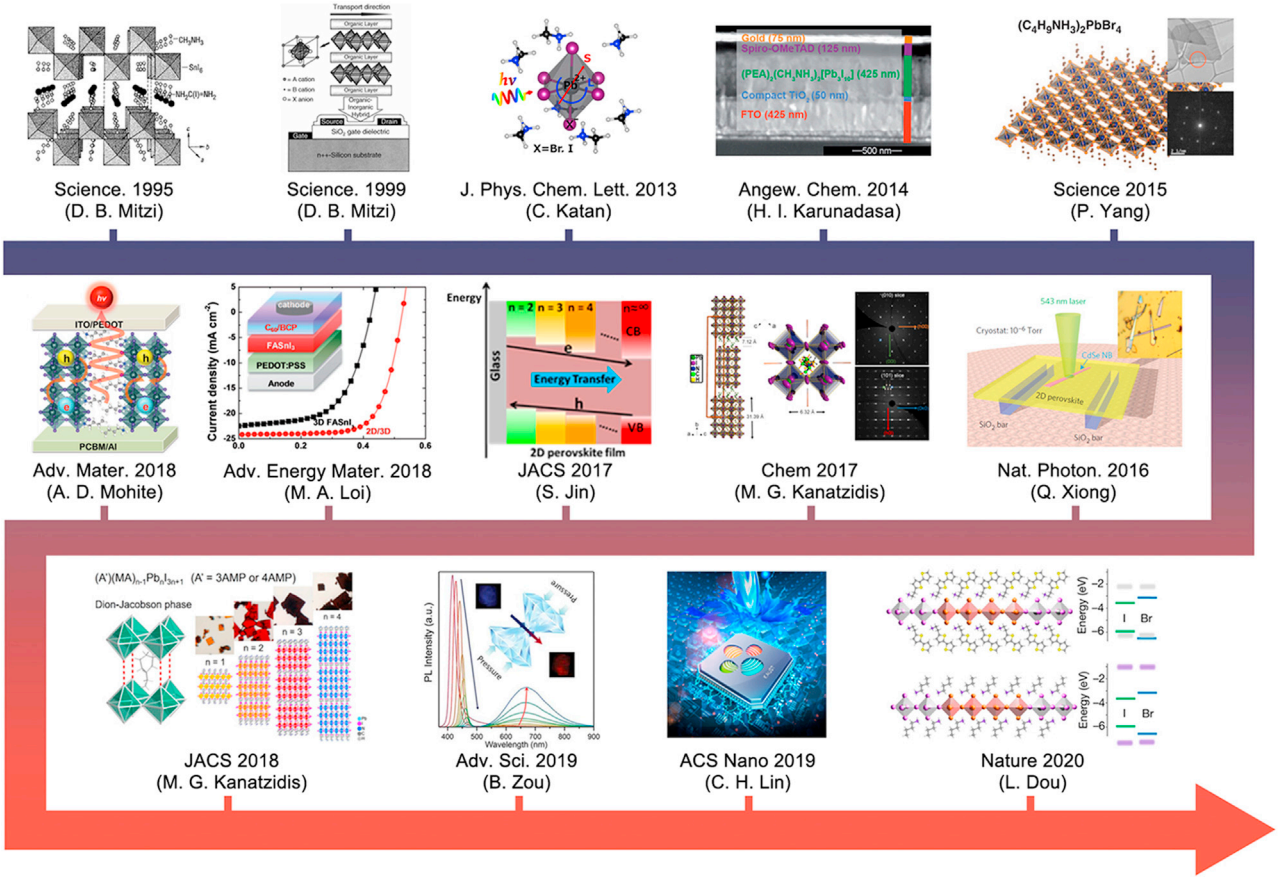

Figure 2. Research timeline of the developments in 2D HOIPs

Reproduced with permission (Mitzi et al., 1994). Copyright 1995 AAAS. Reproduced with permission (Kagan et al., 1999). Copyright 1999 AAAS. Reproduced with permission (Even et al., 2013). Copyright 2013 American Chemical Society. Reproduced with permission (Smith et al., 2014). Copyright 2014 Wiley-VCH. Reproduced with permission (Dou et al., 2015). Copyright 2015 AAAS. Reproduced with permission (Ha et al., 2016). Copyright 2016 Nature Publishing Group. Reproduced with permission (Stoumpos et al., 2017). Copyright 2017 Cell Press. Reproduced with permission (Liu et al., 2017a). Copyright 2017, American Chemical Society (Mao et al., 2018). Copyright 2018 American Chemical Society. Reproduced with permission (Shao et al., 2018). Copyright 2018 Wiley-VCH. Reproduced with permission (Zhang et al., 2019a). Copyright 2019 Wiley-VCH. Reproduced with permission (Lin et al., 2019). Copyright 2019 American Chemical Society. Reproduced with permission (Shi et al., 2020). Copyright 2020 Springer Nature Ltd.

Synthesis of 2D HOIP

Solution methods

In recent years, some representative techniques have been used to prepare 2D HOIPs materials. The most efficient and convenient preparation methods can be divided into two categories, namely solution and vapor methods. The solution method is one of the main preparation methods of 2D HOIPs that are widely accessible using low temperature deposition techniques. The basic procedure is essentially to gently add metal halides and organic ammonium salts into the cosolvent, and after sufficient reaction time, 2D HOIPs samples can be obtained by dry casting or aging procedure, as shown in Figure 4A. Dou et al. obtained atomically thin 2D HOIPs [$(C_4H_9NH_3)_2PbBr_4$] and derivatives by growing directly from solution (Dou et al., 2015). A ternary cosolvent was used to synthesize uniform square-shaped 2D crystals with high yield and excellent reproducibility on a flat substrate, as shown in Figures 4B and 4C. Following the same recipe, Chen and coworkers employed a chlorobenzene-dimethylformamide-acetonitrile ternary solvent method to prepare the 2D $(C_4H_9NH_3)_2PbBr_4$ perovskites (Chen et al., 2017a). A larger lateral dimension and smaller thickness of a few nanometers were obtained. The critical factors, including the influence of solvent volume ratio, solvent polarity, and crystallization temperature on the growth dynamics were systematically studied. It is found that the combined effects of c-axis suppression and diffusion-mechanism-dominated branched growth determine the 2D HOIPs framework.

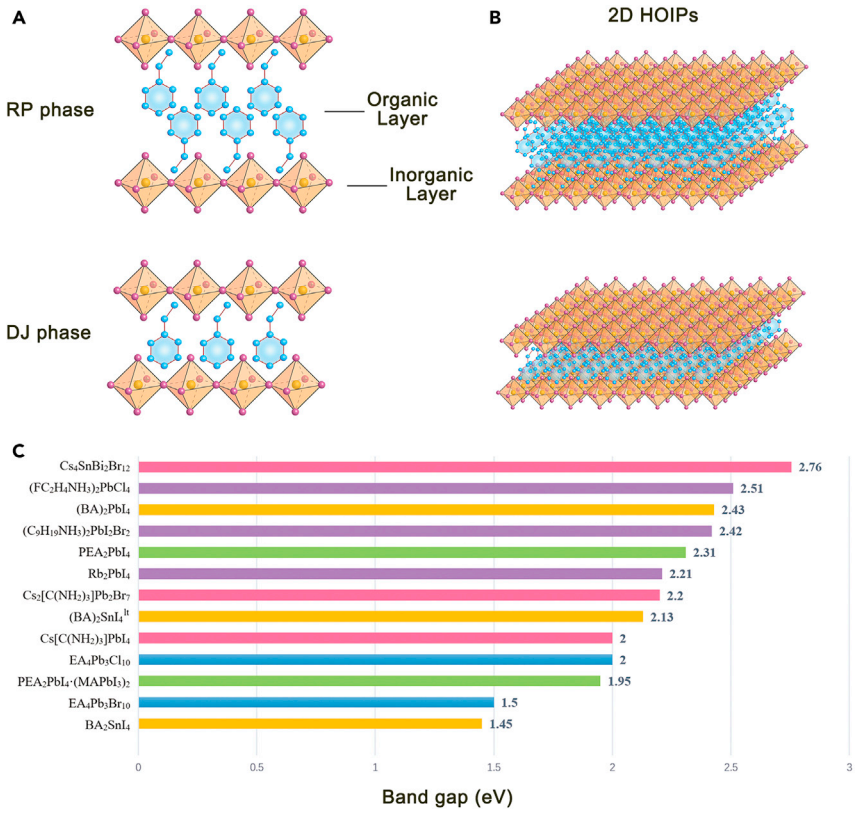

Figure 3. Structure information of 2D HOIPs

(A) Structures and (B) schematic of the 2D HOIPs.

(C) Summary of bandgap energy of typical 2D HOIPs. $(BA)_2PbI_4$ (Stoumpos et al., 2016), BA_2SnI_4(Chen et al., 2017a), $(FC_2H_4NH_3)_2PbCl_4$ (Lermer et al., 2016), PEA_2PbI_4(Peng et al., 2017a), $PEA_2PbI_4{\cdot}(MAPbI_3)_2$ (Peng et al., 2017b), $Cs_4SnBi_2Br_{12}$(Xu et al., 2018b), $EA_4Pb_3Br_{10}$(Mao et al., 2017a), $EA_4Pb_3Cl_{10}$(Mao et al., 2017a), $(C_9H_{19}NH_3)_2PbI_2Br_2$(Abid et al., 2017), $Cs_2[C(NH_2)_3]Pb_2Br_7$ (Nazarenko et al., 2017), $Cs[C(NH_2)_3]PbI_4$ (Nazarenko et al., 2017), Rb_2PbI_4(Guo et al., 2017b), $(BA)_2SnI_4$(Wang et al., 2018)

Apart from the solution methods mentioned above, colloidal synthesis can be an alternative approach reported by Schmidt et al. (Schmidt et al., 2014). In addition, Tyagi et al. managed to obtain 2D monolayer methylammonium lead bromide perovskite ($CH_3NH_3PbBr_3$) crystal using colloidal method (Tyagi et al., 2015). In their works, lead bromide and methylammonium bromide were dissolved in dimethylformamide; subsequently, the mixture was added into a toluene solution to obtain a colloidal solution of $CH_3NH_3PbBr_3$ nanostructures. It turns out that the PL emission peak was blue-shifted about 0.5 eV from the sharp excitonic absorption feature of the bulk $MAPbBr_3$ phase, confirming the feature of 2D nanostructure.

Perovskite nanoplatelets with different thicknesses can be acquired via adjusting the ratio of organic cations used in the synthesis, namely octylammonium and the shorter methylammonium. The layer thickness of the product was decreased as the content of octylammonium in the precursor suspension increased. Similar method was employed to synthesize $CH_3NH_3PbBr_3$ nanosheets with different layers (Huang et al., 2017). Zhong and his coworkers proposed the synthesis of uniform $CH_3NH_3PbBr_3$ nanoplatelets through the self-organization method of preformed colloidal $CH_3NH_3PbBr_3$ nanodots (Figures 4D and 4E) (Liu et al., 2017b). Maintaining the obtained colloidal nanocrystals at 3.5 mg/mL (a high concentration) for three days or combining the synthesis of nanodots with self-organization for tailoring the geometric transformation from spherical nanodots to square or rectangular nanoplatelets. These findings highlight successful examples in the preparation of 2D HOIPs nanoplatelets.

2D HOIPs can be grown by the noncolloidal approaches to tailor a well-defined thickness (the value of "n") and large lateral dimensions. However, the drawback of this approach is lack of process ability after material deposition. Moreover, it is difficult to transfer the as-deposited samples to other desired substrates. In

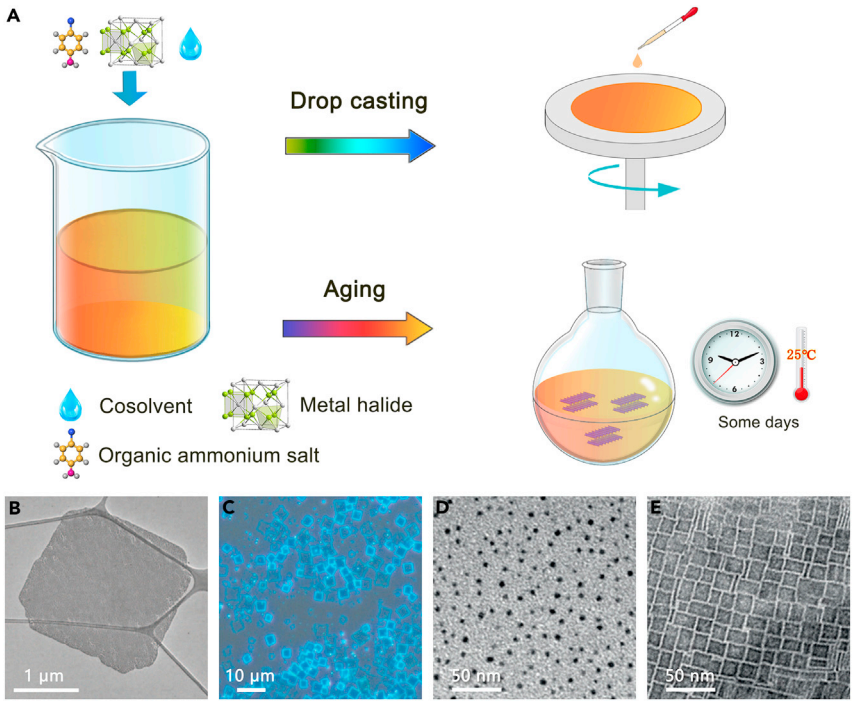

Figure 4. Preparation of 2D HOIPs using a solution method

(A) Solution-based synthesis schematic of 2D HOIPs.

(B) TEM image of $(C_4H_9NH_3)_2PbBr_4$ sheets.

(C) Optical image of the 2D square sheets. Reproduced with permission (Dou et al., 2015). Copyright 2015 American Association for the Advancement of Science. And TEM images of the $CH_3NH_3PbBr_3$ nanodots (D) and the resultant nanoplates (E). Reproduced with permission (Liu et al., 2017b). Copyright 2017 Wiley-VCH

comparison to the noncolloidal chemistry, the colloidal methods offer facile and fast routes to synthesize 2D HOIPs. However, the as-synthesized 2D HOIPs based on colloidal solution method can be difficult to control their thickness and lateral dimensions size. Therefore, significant attempts have been made to improve the output of colloidal approaches. For instance, by changing the HBr amount, the ligand amount, and their ratio, the temperature of the synthesis, the reaction time, as well as the length of ligands, the morphologies of 2D HOIPs can be varied, so that the thickness-dependent and size-dependent properties are characterized. In the aforementioned wet chemistry approaches, surfactant plays an important role to accommodate morphology improvement during the synthesis process. However, a surfactant could contaminate the surface materials and eventually negatively influences the intrinsic electronic properties of 2D materials.

Vapor methods

The vapor method includes diverse and versatile deposition techniques, namely, the chemical vapor deposition (CVD), and van der Waals epitaxy is one of the most widely explored approach for other 2D materials such as grapheme (Lang et al., 2015; Wang et al., 2011), transition metal dichalcogenides (TMDs) (Jiang et al., 2017; Qi et al., 2017; Suleiman et al., 2020; Zhang et al., 2019b), and 2D transition-metal carbides/nitrides, and carbonitrides (MXenes) (Xu et al., 2015). It is also applied in the growth of perovskite thin films (Lewis and O'Brien, 2014; Leyden et al., 2014). Ha and his coworkers synthesized the organic-inorganic lead halide perovskite nanoplatelets with a two-step vapor method (Ha et al., 2014). First, the PbI_2 nanoplatelets on the surface of muscovite mica were prepared in a vapor transport chemical deposition system utilizing van der Waals epitaxy.

The as-grown platelets were transformed to $CH_3NH_3PbI_3$ perovskites through a gas-solid hetero-phase reaction with methylammonium halide molecules. The schematic of this method with the vapor-transport system is shown in Figure 5A. The color of the lead halide platelets can be tuned as a function of thickness. The thickness of PbI_2 platelets had a linear relationship with the $CH_3NH_3PbI_3$ platelets, whereby the ratio

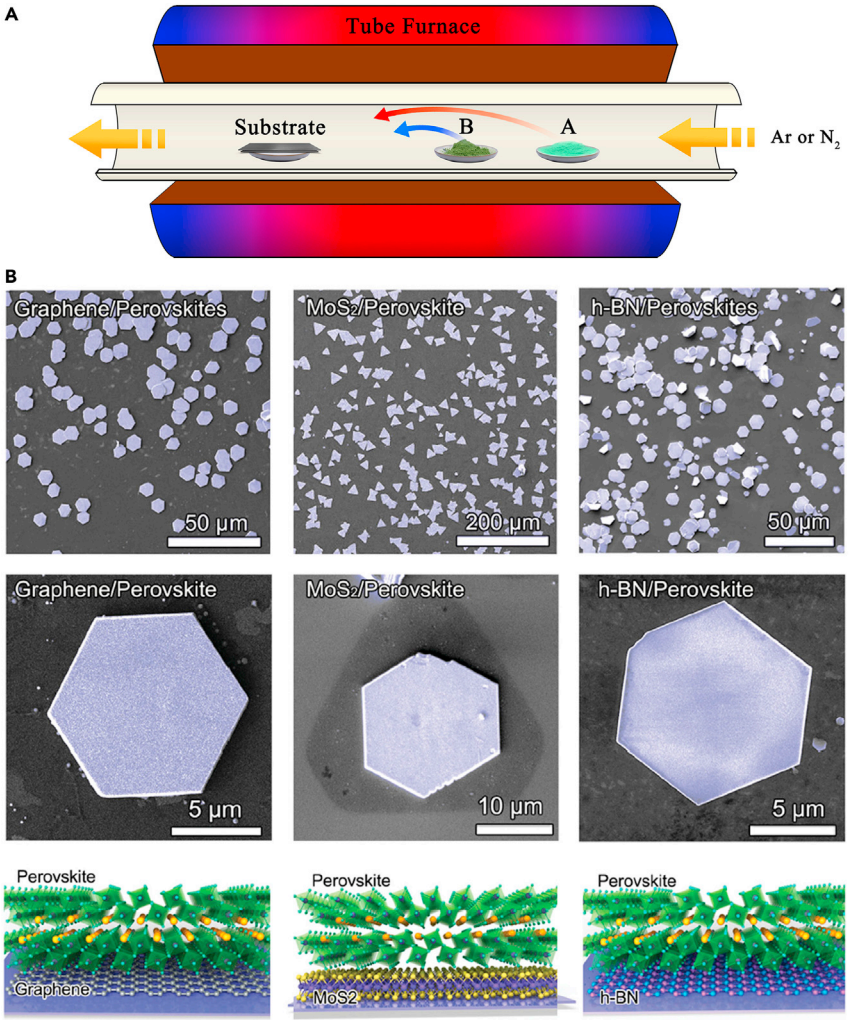

Figure 5. Preparation of 2D HOIPs using a vapor method

(A) Schematic of the preparation of 2D HOIPs by vapor methods.

(B) Morphologies of the perovskite/2D van der Waals (VDW) solids probed by scanning electron microscopy. Reproduced with permission (Niu et al., 2015). Copyright 2015 Wiley-VCH

follows the *c* lattice constant variation. Liu group has made significant contributions to the development of the vapor synthesis of 2D HOIPs(Niu et al., 2015). In 2015, organic/inorganic van der Waals solids that consist of perovskite and some other 2D materials such as graphene, MoS_2, and hexagonal boron nitride (*h*-BN) with CVD were fabricated (Figure 5B) (Niu et al., 2015).

In the following years, 2D $CH_3NH_3PbI_3$ microplatelet arrays and $CH_3NH_3PbI_3$ nanoplatelets on the silicon substrate with single layer *h*-BN film as the buffer layer were successfully synthesized (Liu et al., 2016; Niu et al., 2016). The *h*-BN film acted as not only the intermediate layer, but also as the growth nuclei site. By changing the synthesis condition, the thickness of nanoplatelets is controllable between a few layers to hundred nanometers. Wang et al. prepared 2D $MAPbCl_3$ perovskite with operating temperature at 220°C using the dual precursor sources CVD method (Wang et al., 2015b). In their study, the fractal evolution of $MAPbCl_3$ thin films and the VDW epitaxy mechanism was explained in combination with Monte Carlo simulations. It is the weak interaction of the VDW film with the substrate and the low cohesive energy of the perovskite halide that make large-scale growth of single crystal ultrathin 2D crystals possible.

When it comes to the all-inorganic metal halide perovskites, it is not feasible to use vapor methods for the synthesis, because of their strong covalent bonding and non-van-der-Waals characterization. However,

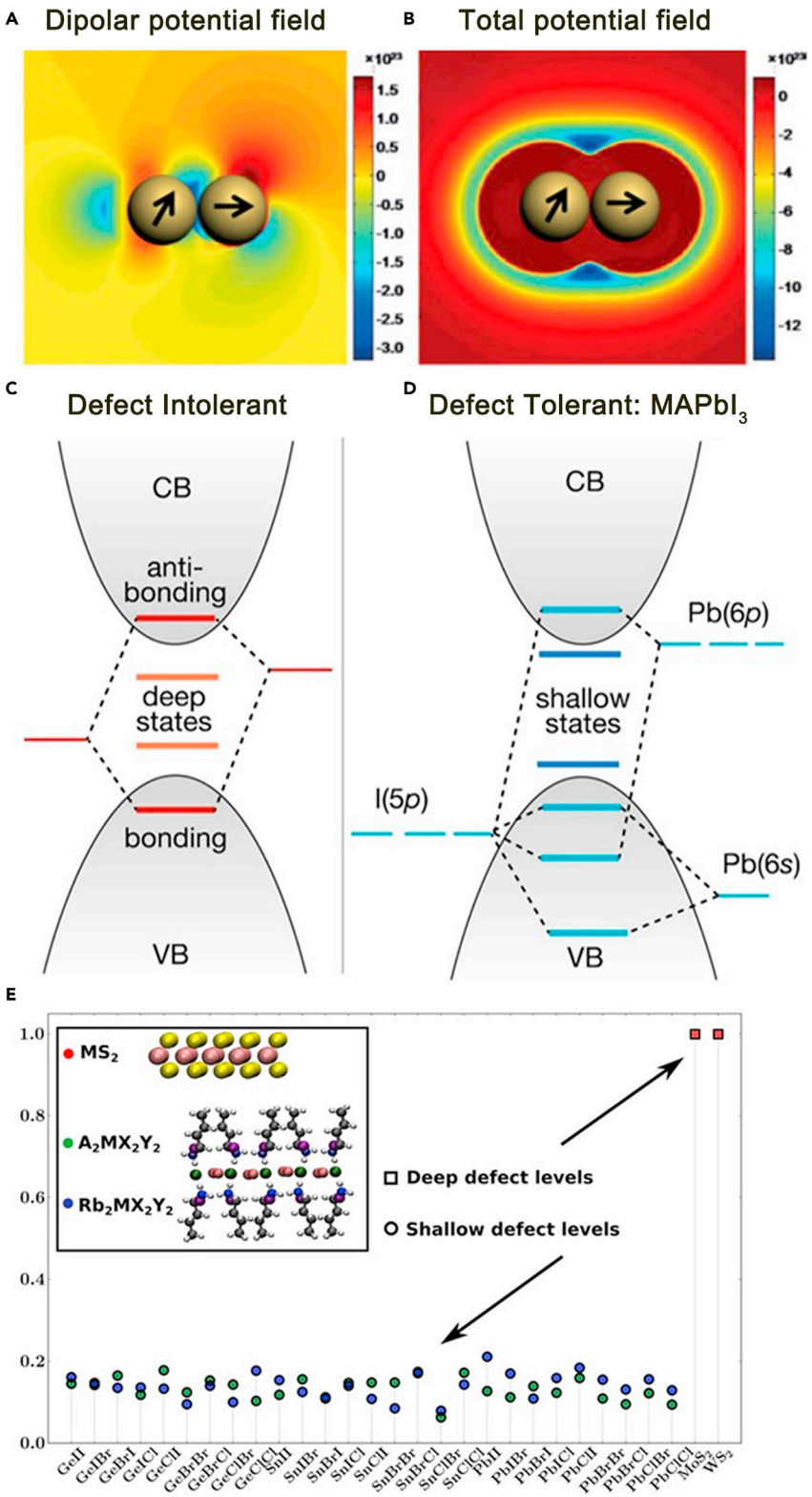

Figure 6. Defect state analysis of halide perovskite

(A and B) The potential field distribution in a two dot alignment of $CH_3NH_3PbBr_3$ NCs(Liu et al., 2017b). (C) Electronic structure of typical III-V, II-VI, or group IV defect intolerant semiconductors compared to (D) the defect tolerant lead halide perovskite (Brandt et al., 2017).

Figure 6. *Continued*
(C and D) are reproduced with permission from ref (Brandt et al., 2017). Copyright 2017, American Chemical Society.
(E) Normalized orbital overlap (NOO) to describe the similarity of the states near the band edges (Pandey et al., 2016). (E) is adapted with permission from ref (Chen et al., 2019b). Copyright 2016, American Chemical Society

Zhang et al. successfully synthesized $CsPbX_3$ (X = Cl, Br, I) via VDW epitaxy method (Zhang et al., 2016). This serves as a generic recipe of vapor methods in all-inorganic metal halide perovskites fabrications (Hu et al., 2017; Wang et al., 2017a; Zhou et al., 2017). Compared with solution methods, the 2D HOIPs structures prepared by CVD or VDW epitaxy method have shown good crystallinity and high purities. It is noted that Chen et al. developed a self-doping approach for preparing ultrathin and large sized 2D homologous $(C_4H_9NH_3)_2(CH_3NH_3)_{n-1}Pb_nBr_{3n+1}$ perovskites by using 2D $(C_4H_9NH_3)_2PbBr_4$ perovskites as a template with $CH_3NH_3^+$ dopant by incorporating both solution and vapor methods (Chen et al., 2017b). In the first step, the 2D $(C_4H_9NH_3)_2PbBr_4$ perovskites were obtained by ternary solvent method. Transformation of 2D $(C_4H_9NH_3)_2PbBr_4$ into 2D homologous $(C_4H_9NH_3)_2(CH_3NH_3)_{n-1}Pb_nBr_{3n+1}$ perovskites was implemented by CVD of CH_3NH_3Br. Interestingly, it took the advantages of both solution and vapor methods by changing the direction of source vapors and carrier gas flow, which can selectively oxidize and etch the unstable nuclei and edges. Hence, realizing continuous domain size and sequential edge-epitaxy growth is required to promote the controllable synthesis of high-quality 2D materials.

Among the two main types of preparation methods, the solution method, in which the reactants are added directly to the cosolvent for reaction, can synthesize two-dimensional crystals with high yields and good reproducibility because of its less demanding reaction conditions. In addition, by changing the reaction conditions to influence the growth kinetics, larger size, and smaller thickness of the material can be obtained. However, the addition of solvents inevitably contaminates the surface material and affects the properties. In contrast, good crystallinity and high purity of 2D crystals can be obtained by the vapor method, but the thin film materials prepared by the conventional vapor method tend to be thicker, so researchers have made it possible to synthesize thinner and larger 2D crystals by adding VDW epitaxy method.

Theoretical designing

Material design by DFT calculations holds a predominant role in the study of the physicochemical properties of hybrid perovskites. From theoretical constructions and calculations of the expected crystal structure, we can effectively predict their possible performances, and provide a systematic guidance on how to synthesize the desired structures, explain the growth process, and to analyze the intrinsic feature of the device performance.

The strong spin-orbit coupling effect cannot be neglected in these halide perovskites as they could manifest as about 1 eV to the bandgap, while the underestimated bandgap energy through the LDA method has similar value. In 2016, Kanatzidis et al. (Stoumpos et al., 2016) first reported the crystal, electronic structures and optical properties of $(BA)_2(MA)_{n-1}Pb_nI_{3n+1}$ HOIPs with varied n value. The results revealed that by increasing n value, the bandgap energy decreases. The particular perovskites exhibit promising PL features when the value of n is smaller than 2, on the other hand, this characteristic is not appealing for photoelectric applications. When the n is larger than 3, these perovskites cover the visible range of solar energy, leading to a huge potential in the conversion of visible light irradiation into electric energy. There are several classes of hybrid perovskites that are potentially promising candidates for photovoltaics. Fundamental criteria of the electronic properties of monolayer HOIPs of BA_2MI_4 (M = Pb, Ge, or Sn) have been investigated by DFT with Heyd-Scuseria-Ernzerhof (HSE) functional level (Ma et al., 2017). In the calculation result, the bandgap of 2D BA_2MI_4 is found to be 1.5–2.0 eV, whereas the ultrathin 2D BA_2GeI_4 and BA_2SnI_4 show the bandgap energy of 1.7 and 1.5 eV, respectively.

In 2017, Stoumpos et al. (Stoumpos et al., 2017) have successfully synthesized $(CH_3(CH_2)_3NH_3)_2(CH_3NH_3)_4Pb_5I_{16}$ in high yield and purity. In addition, a computational calculation of the corresponding electronic structure is presented. The inclusion of spin-orbital coupling (SOC) gives rise to the conduction band lifting that consequently lowered the bandgap of 0.28 eV located at Γ(Stoumpos et al., 2017). In addition, the flat dispersions along the Z-Γ and *Y*-Γ directions in the reciprocal space suggest the nature of layered structure and the absence of electronic coupling between interlayers, reflecting the 2D nature of the hybrid materials.

In the process of preparing 2D $CH_3NH_3PbBr_3$ by colloidal approach, Zhong et al. (Liu et al., 2017b) used DFT to study the self-assembly process of hybrid perovskites (Figure 6A). Two and four coalescent

nanodots (NDs) have the most stable structure during the self-organization process by taking into consideration of the variation of dipolar vectors (Liu et al., 2017b). As such, a wide range of studies systematically investigated the function of organic groups by the DFT method. Since the organic ligands could serve as a dominant role in determining the dynamic structure of halide perovskites, it is quite difficult to unambiguously determine the precise position of organic groups because of the random orientation. Defect can be unintentionally generated during structural transformation from bulk perovskites into 2D HOIPs. Owing to the nature of layered structure, 2D HOIPs introduce more defects that can be related to the grain boundaries, which act as recombination centers and thereby decrease the PL quantum yield and charge carrier lifetime (Iyikanat et al., 2017). Therefore, extended studies have been focused to understand the implication of defects in the 2D HOIPs-based device performance.

The nature of defect-tolerance of bulk halide perovskites has been well studied (Brandt et al., 2017; Shi and Du, 2014; Yin et al., 2014). Specifically, the contribution of defect-tolerance to the perovskite performance is investigated. The following factors are important to consider: the mixed ionic-covalent bonding (related to the large Born effective charges and high dielectric constant) (Du, 2014; Du and Singh, 2010; Park et al., 2019), excess of halogen (Srimath Kandada et al., 2016), insufficient cation orbital hybridization at halogen vacancies (with large interionic distance for cation and low coordination numbers for anion) (Shi and Du, 2014), small capture cross sections (with low charge states) (Brandt et al., 2017). The cations with the outermost electron configuration of ns^2 (*i.e.* Tl^+ and Pb^{2+}) has a significant contribution to the shallow defect states in halide perovskites (Figures 6C and 6D) (Brandt et al., 2017). Using the normalized orbital overlap (NOO), Pandey quantitatively described the tendency to form mid-gap defect states and this feature resembles the electronic states near the band edges (Pandey et al., 2016). As shown in Figure 6E, the NOO values of different perovskites are significantly less than 1, which indicates the shallow defect levels within the bandgap for optimizing device performance (Pandey et al., 2016).

Energy applications

At present, there are many challenges in the development of various subfields in the energy field, such as the improvement of photoelectric conversion efficiency in the photovoltaic field, the balance between the reaction rate and reaction speed of photodetectors, and the joint improvement of supercapacitor capacity and discharge efficiency. In addition, there are some common problems such as stability. Among many exciting characteristics of 2D HOIP, the excellent optoelectronic properties, such as the large absorption coefficient, high carrier mobility, and long diffusion length, make them promising for energy applications. Up to now, great achievements have been made in various energy utilizations. Here, we summarize the recent progress of 2D HOIP for energy applications, including photovoltaics, and photodetectors, supercapacitor, LEDs, and Thermoelectricity.

Photovoltaics and photodetectors

In a short period of time, HOIP based solar cells have been significantly improved in terms of power conversion efficiency (PCE) from 3.8% to 25.6% (Jeong et al., 2021). After the boom of research in photovoltaic, breakthroughs were subsequently achieved in a range of energy conversion and storage fields such as light-emitting diodes (LEDs), supercapacitor, thermoelectric. Despite the recent spectacular progress and development, most of the devices based on HOIP with 3D crystal structures suffer from degradation caused by ion migration, high temperature, UV irradiation *etc.*, which poses a challenge for the future commercialization. 2D HOIPs have significant advantages in comparison with their 3D counterpart not only in the superior stability but also in the higher structural diversity. However, 2D HOIPs with n = 1 have a considerably large bandgap (>2.0 eV), high exciton binding energy (~300 meV), and strong electron–phonon coupling, which hampered its photovoltaic applications.

Herz et al. (Herz, 2017) described the underlying mechanism that defined the basic upper limit to charge-carrier mobility values in MHPs. This parameter can be adjusted by changing their stoichiometric number, n. They reported that the effective charge-carrier mobility generally decreased with increasing 2-phenylethylammonium (PEA^+) content, with a trade-off between electronic confinement and layer orientation, the effective charge-carrier mobility of quasi-2D HOIP $MA(PEA)_2PbI_7$ can reach a maximum of 11 $cm^2/(V.s)$.

Recently, significant progress have been made in terms of the efficiency of quasi-2D HOIP based solar cells (Zhang et al., 2021), *i.e.*, over 19% for the Ruddlesden–Popper phase, 18% for the Dion–Jacobson phase and the alternating cations in the interlayer space phase. Controlling the crystallographic planes of the

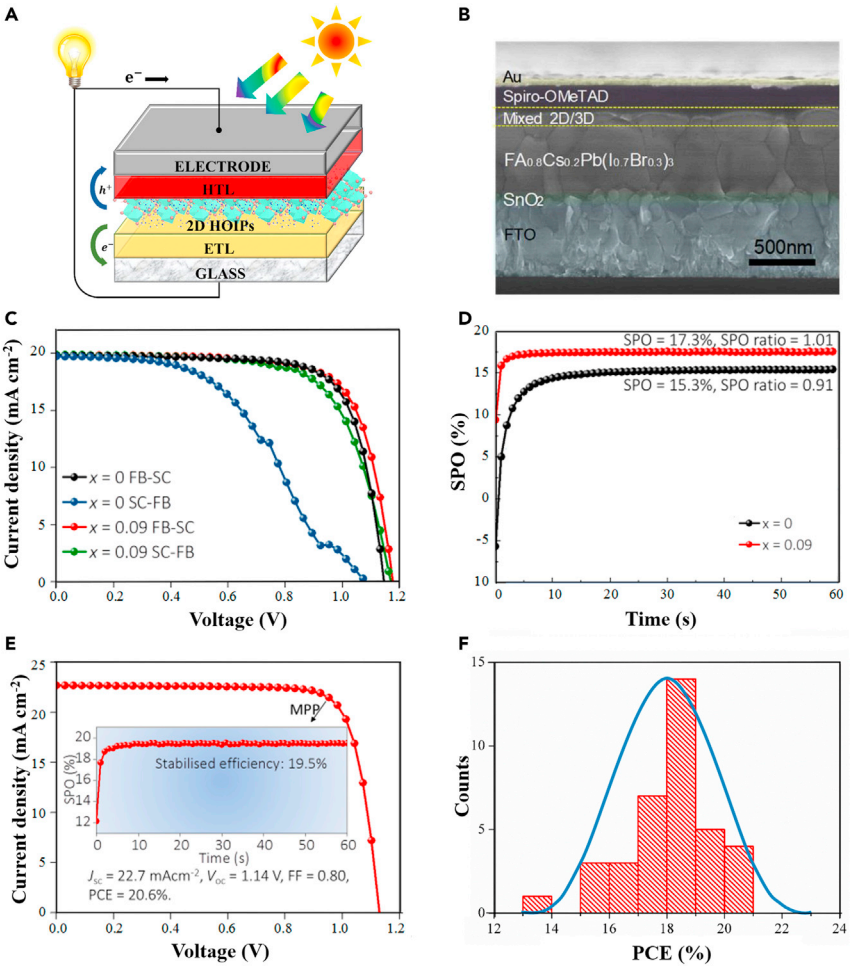

Figure 7. The application and performance of 2D HOIPs in the field of photovoltaics

(A) Schematic of 2D HOIPs solar cells.

(B) Cross-sectional SEM image of PSCs with 8 mg/mL PMABr/IPA solution treatment. Reproduced with permission (Bu et al., 2020). Copyright 2020 Elsevier Ltd.

(C) J-V characteristics of optimized perovskite solar cells with different active layers.

(D) Stabilized power output (SPO) of the champion cells.

(E) J-V characteristic of the best performing perovskite solar cells, and (F) the distribution of PCE. (E-F) are adapted and modified with permission from ref (Wang et al., 2017b). Copyright 2017 Nature Publishing Group

inorganic layer with a preferential vertical alignment, and optimization of the thickness distributions of QWs within the film are two most effective ways to improve the efficiency of quasi-2D perovskite solar cells. For example, cation engineering on mixed halide perovskite is shown in Figures 7C–7F n-Butylammonium cation was introduced into a mixed-cation bulk perovskite $FA_{0.83}Cs_{0.17}Pb(I_yBr_{1-y})_3$, which was synthesized by Wang and coworkers (Wang et al., 2017b).

The formation of 2D HOIPs, interspersed among highly orientated bulk perovskite grains, which resulted in suppression of the nonradiative charge recombination. Moreover, the solar cells measurements indicated that an optimum butylammonium content led to average stabilized PCE of 18% with a 1.61 eV-bandgap perovskite, as shown in Figures 7C–6F. The stability under simulated lighting was also improved. In addition, after 1,000 h use of solar cells in the air, their 'post burn-in' efficiency can be well-maintained at about 80% of the initial, and the lifespan after encapsulating is close to 4,000 h.

Xiao and coworkers used materials synthesis, characterization, and DFT calculation methods to explore the photovoltaic characteristics of the 2D $MA_2Pb(SCN)_2I_2$ ($MA = CH_3NH_3^+$) perovskite of $MA_2Pb(SCN)_2I_2$. These

hybrid perovskites are significantly different from those reported in the previous literature (Xiao et al., 2016). Another work by Chen and coworkers has shown a similar theory that a strong vertical orientation is necessary to achieve a reliable solar cell performance (Chen et al., 2018). They fabricated thin films of $BA_2MA_3Pb_4I_{13}$ (BA = butylammonium, MA = methylammonium) by use of a simple solution treatment on various substrates at a temperature ranging from 25 to 140°C. The *ex situ* grazing incidence wide angle X-ray scattering (GIWAXS) results show, depending on the processing conditions, there are different degrees of preferential vertical orientation. The solar cells performance test indicated that $BA_2MA_3Pb_4I_{13}$ with higher degree of vertical orientation manifest higher PCE than those perovskites with randomized orientations. Furthermore, systematically designed *in situ* GIWAXS experiments confirmed that the heterogeneous nucleation and growth of $BA_2MA_3Pb_4I_{13}$ happen to the liquid-air interface, forming a top-crust with strong vertical direction. As such, insights into the self-assembly of 2D metal halide perovskite and its influence on the performance of optoelectronic devices will remarkably promote the wide application of 2D metal halide perovskites devices.

In spite of the notable stability enhancement and efficiency improvement, the PCEs of PSCs based on 2D or quasi-2D perovskite are far from performance of the 3D perovskite and still not sufficient for commercial applications. Recently, a 3D/2D bilayer perovskite structure, in which 2D perovskite is deposited on the 3D bulk film in the form of an extremely thin layer (Figure 7B) have been comprehensively employed to ensure a superb performance in terms of both the stability and PCE of PSCs. Huang et al. achieved an efficiency of 18.5% with negligible hysteresis and a stabilized efficiency of 17.9% for a PSCs based on wide bandgap (~1.74 eV). In addition, the long-term stability of the devices is also remarkably enhanced as no degradation was observed after the devices are stored under ambient air conditions with 20% RH without encapsulation over 2000 h (Bu et al., 2020).

The first photodetector based on 2D HOIPs was successfully manufactured by Tan et al. (2016) Figure 8C shows the current-voltage (ISD-VSD) curves of the device in darkness and different illumination intensities. Here, the photocurrent of the device was gradually increased with the incident power. This 2D HOIPs crystal photodetector exhibits extremely low dark current with graphene gapped electrodes, indicating the good reliability of the perovskite photodetector performance. However, the electroluminescence efficiency of 2D HOIPs is limited by the presence of undesired nonradiative recombination effect, which is related to imperfection and leakage current caused by incomplete surface coverage.

Light-emitting devices

Light emission is a key property that needs to be controlled to achieve high performance in a variety of energy conversion devices including solar cells, LEDs, and lasers. HOIP have superior electrical and optical properties, which offer them great potential for use in LEDs. Their narrow emission linewidths (full width at half maximum (FWHM) $\leq$ 20 nm) can achieve ultra-high color purity (color gamut $\geq$140% in National Television Standards Committee (NTSC) TV color standard), which are superior than traditional light-emitting technologies such as inorganic quantum-dot LEDs (QLEDs, FWHM >40 nm; color gamut <100% in NTSC) and organic LEDs (OLEDs, FWHM $\approx$30 nm; color gamut $\approx$100% in NTSC) (Kim et al., 2019b).

In addition to the property needed for high performance solar cells, such as excellent charge transport properties and large mobilities entail, a key requirement for high performance LEDs is that the charges must be locally confined within the perovskite emissive layer to enhance radiative recombination. Owing to the strong quantum and dielectric confinement that offered by the disruption of the normally periodic perovskite lattice with bisecting organic layers, 2D HOIP can possess exceptionally high exciton binding energy and radiative recombination rate that for high performance LEDs (Walters et al., 2020). Therefore, the PL efficiency of 2D HOIP solids has been increased to near unity and EQE_{max} over 20% of pero-LEDs in the green, red, and infrared light regions (Wei and Xing, 2019).

The structure of 2D HOIPs optoelectronic devices is in principle similar to the aforementioned discussion on solar cell devices. Typically, a light-emitting hybrid perovskite emission diode consists of the positive and negative electrodes, protons and electron transport layers, and 2D HOIPs situated at the middle of device structure as "reaction vessels". The confinement of the 2D structure allows protons and electrons to recombine more efficiently between layers to produce photons as shown in Figure 8A(Kim et al., 2015).

Wang et al.(Ishihara et al., 1989) demonstrated a solution-processed perovskite light-emitting diode (LED) device based on self-organized multiple quantum wells (MQWs). It has eminent film morphology, and its

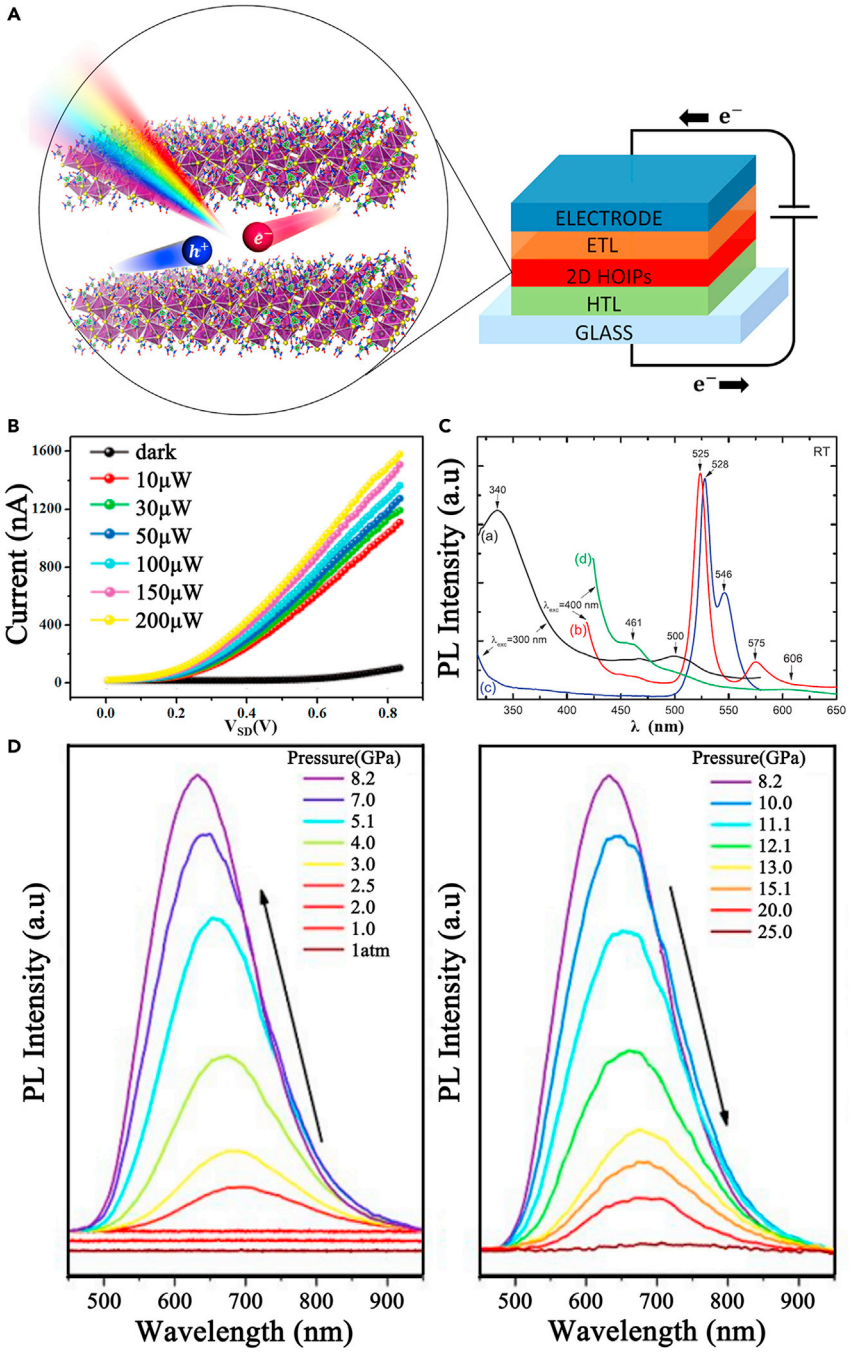

Figure 8. 2D HOIPs in Light-emitting devices

(A) Schematic of 2D HOIPs LED device.

(B) Current-voltage (I_{SD}-V_{SD}) curves under different illumination intensities. Reproduced with permission (Tan et al., 2016). Copyright 2016 American Chemical Society.

(C) PL spectra of corresponding 2D HOIPs. Reproduced with permission (Papadatos et al., 2017). Copyright 2017 Elsevier.

(D) PL spectra of $(BA)_4AgBiBr_8$ at high pressure. Reproduced with permission (Fang et al., 2019). Copyright 2019 Wiley-VCH.

external quantum efficiency is as high as 11.7%, which is extremely stable. When the current density is 100 mA cm^{-2}, the energy conversion efficiency is 5.5%, signifying excellent high-power performance. The perovskite MQWs with higher energy gap effectively drive these excellent optoelectronic performances, thereby producing effective radiation decay characteristics.

Recently, it was discovered that because of the self-trapped excitons (STEs), within the visible range, 2D HOIPs exhibited white-light and broadband emission. Mao and coworkers incorporated the bifunctional ammonium di-cations to 2D lead bromide perovskites that serve as templates for white light emitter applications (Mao et al., 2017b). Moreover, the corresponding PL research shows that the inorganic layer is directly related to the geometrical distortion of the "$PbBr_6$" octahedron. The PL emission broadening indicates that the octahedral distortion of the inorganic layer becomes larger; therefore, the bandwidth of the PL emission is widened. For instance, the most distorted perovskite structure has the widest emission and the service life (T_{avg} = 1.39 ns) (Tan et al., 2016). Among these three compounds, an intriguing "3 × 3" type of corrugated (110)-oriented 2D HOIPs, α-(DMEN)$PbBr_4$, is fixed by "chelating effect", a special effect of hydrogen bonding interactions. Owing to this influence, the distorted structure of α-(DMEN)$PbBr_4$ is the most obvious compared to the other two homologue compounds, resulting in wide white-light emission, and the color rendering index (CRI) is 73. This result is comparable to the fluorescent light source and correlated color temperature (CCT) of 7863 K, and producing "cold" white light. As a whole, this work not only shows a highly efficient white light luminescent material, but also this correlation can be used as a breakthrough for PL emission characteristics in other related 2D HOIPs systems.

Papadatos and coworkers have presented a single layer LED that operates based on the concept of energy transfer effects (Papadatos et al., 2017). Compared to the traditional manufacturing strategy, the proposed work offers an instant, simple, and low cost method (Papadatos et al., 2017). The active LED layer is basically a mixture of 0D $(CH_3NH_3)_4PbI_6$, 2D $(F\text{-}C_6H_4CH_2CH_2NH_2)_2PbI_4$ and 3D-bulk $(CH_3NH_3)PbI_3$ HOIPs that transformed into a quasi-2D HOIPs for the first time. The OA spectra of this quasi-2D structure are shown in Figure 8C. During the electroluminescence behavior, it exhibited peculiar excitonic recombination bright yellow light that centered at a peak of 592 nm. In this scenario, utilizing the proper mixtures ratio to create films containing these phases allows us to demonstrate a multicolor EL emission. Several combinations can be found: yellow/green or yellow/red/deep-red emission. An LED device made under air is beneficial since it can be operated at low voltages and room temperature, whereas the active layer showed considerable film continuity under any deposition method. In addition, the high-efficiency quasi-2D structure perovskite light-emitting diodes (4.90 cd A^{-1}) have been proved to be a mixture of a bulk methylammonium lead bromide and a 2D phenylethyl ammonium lead bromide. Hence, the excellent optoelectronic performance could be attributed to enhanced exciton confinement, excellent film uniformity, and reduced trap density (Byun et al., 2016).

In the investigation of the luminescent properties of 2D HOIPs, the pressure-induced luminescent phenomenon (PIE) has also attracted considerable attention besides the electroluminescent properties. Mao et al. (Fang et al., 2019) have systematically studied the luminescent properties of $(BA)_4AgBiBr_8$ (BA = $CH_3(CH_2)_3NH_3^+$) under certain pressure. The relationship between the PL intensity and frequency is shown in Figure 8D. It was found that with increasing pressure, a broad emission band with FWHM of ~180 nm suddenly appeared at 2.5 GPa. Another excellent work in this field has been reported by Zhang et al. (Zhang et al., 2019a). By exploring layered (001) Pb-Br perovskite pressure-induced broadband emission under different pressures, a new route for adjusting the optical properties of 2D HOIPs was established.

Supercapacitor

Compared to the conventional parallel-plate capacitors, the design of supercapacitors has shown a tremendous capacity output and a faster discharge rate relative to the Li-based batteries. In recent years, researchers have attempted to use 2D HOIPs since their characteristics are promising for supercapacitor applications. Figure 9A shows the device structure using 2D HOIPs as a supercapacitor material. Compared with conventional electrode materials, the 2D HOIPs own higher surface area and better ionic mobility, which make these materials promising for the candidate of electrodes in the design of supercapacitors.

Through impedance spectroscopy, the ionic conductivity in $MAPbI_3$ (MA, methylammonium) can be measured as a value of ~10^{-8} S cm, indicating that the perovskite $MAPbI_3$ was a solid electrolyte with both the transport capacity of ion carrier and electron carrier. Figure 9B shows the measured value of charge densities caused by the ions accumulation at the interfaces under different biases, and the capacitance could be calculated from the slope of the curve. Having a large capacitance (~100 μF cm^{-2}) and EMF (open-circuit electromotive force ~0.5 V), $CH_3NH_3PbI_{3-x}Br_x$ is regarded as a potential energy-storage material that is applicable for the field of solid-state supercapacitors (Zhang et al., 2015).

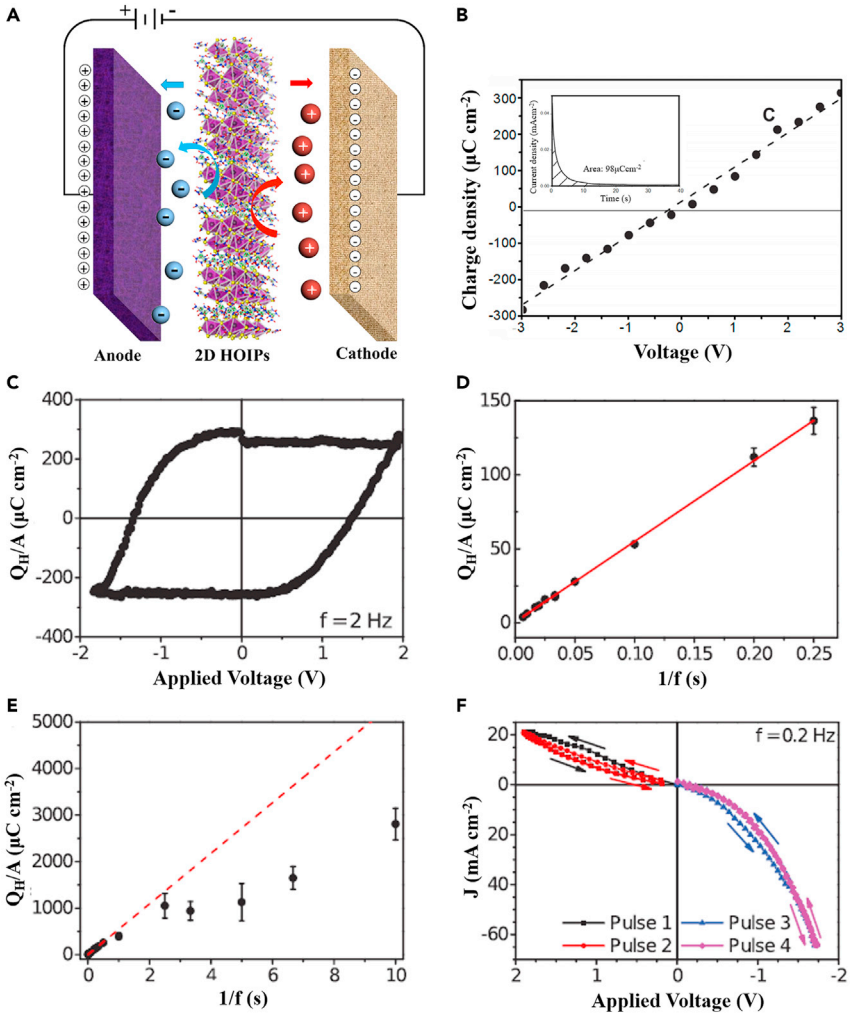

Figure 9. The application and performance of 2D HOIPs in supercapacitors (A) Schematic of 2D HOIPs supercapacitors

(B) Ionic behavior of the perovskite $MAPbI_3$ exhibited prominent interface charge density at various biases. Reproduced with permission (Zhang et al., 2015). Copyright 2015 Wiley-VCH.

(C) Hysteretic charge density (QH/A) as measured by the DWM on a $CH_3NH_3PbI_3$ thin film.

(D and E) Frequency dependence of the QV hysteresis as a function of 1/f. (F) DWM measurement plotted as J-V curves. Reproduced with permission (Beilsten-Edmands et al., 2015). Copyright 2015 AIP Publishing

Based on Beilsten-Edmands' research (Beilsten-Edmands et al., 2015), the ionic motion within the material can be used to determine the capacitance value of ~1.8 mF cm^{-2} in a 350-nm-thick $CH_3NH_3PbI_3$ material in a parallel-plate capacitor (electrostatically). Figure 9C shows the hysteretic loop of thin films at 2 Hz, and the changes of the hysteretic charge density with frequency are shown in Figures 9D and 9E. The shape of the presented loop resembles the ferroelectric material; however, the hysteresis charge density is an order of magnitude greater than that of the perovskite ferroelectric material. To determine the true cause of the QV hysteresis, pulse-based measurements were carried out to verify that the majority of the frequency depends on the current density rather than the accumulated charges (Figure 9F). This finding suggests that the current - voltage hysteresis is not driven by the ferroelectricity, which further highlights the significance of ionic migration to improve the efficiency of $CH_3NH_3PbI_3$ devices.

Thermoelectricity

Thermoelectricity is another form of energy conversion to transfer waste heat into electricity. To date, various metal halide perovskites have been employed as active material in the thermoelectric fields.

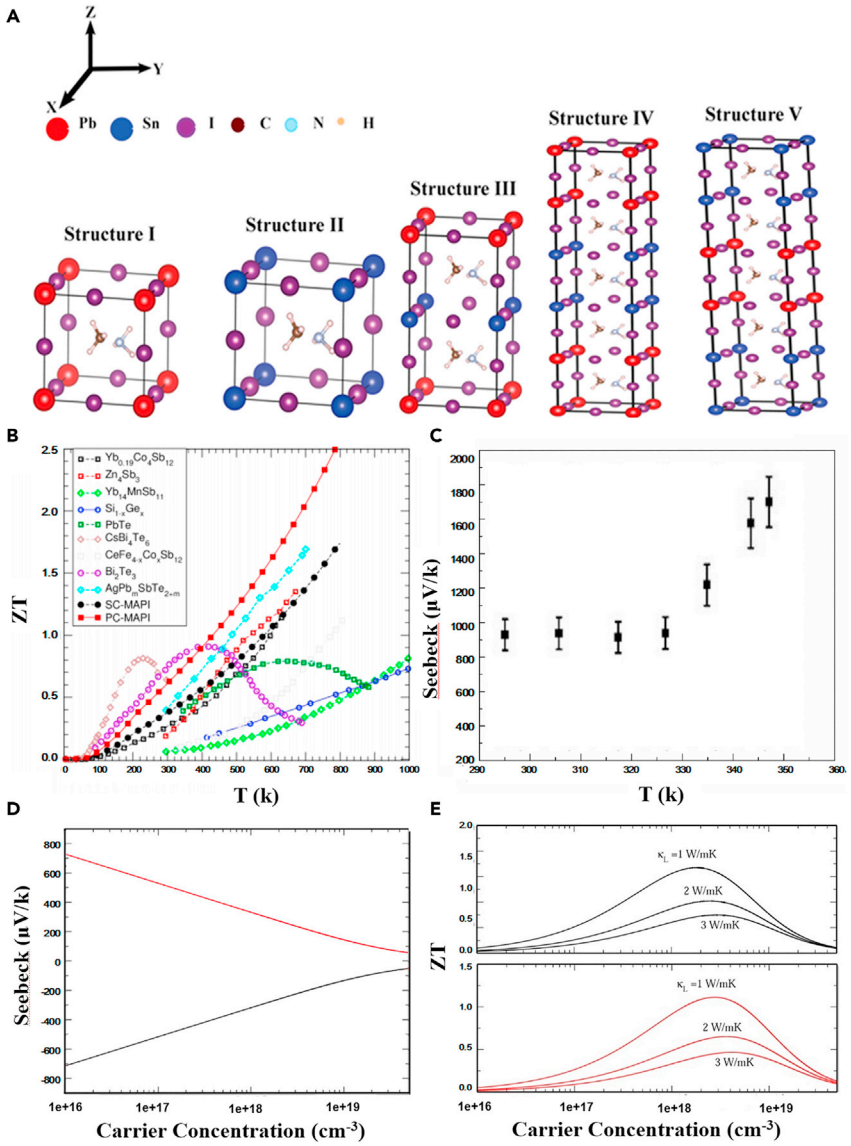

Figure 10. The thermoelectric performance of HOIPs

(A) Molecular representation of the different HOIPs structures. Reproduced with permission (Singh et al., 2017). Copyright 2017 Royal Society of Chemistry.

(B) Comparison of the thermoelectric properties of *n*-doped SC and PC $MAPI_3$ with other thermoelectric materials with the best performance. Reproduced with permission (Filippetti et al., 2016). Copyright 2016 American Chemical Society.

(C) Seebeck coefficients of centimeter-sized $CH_3NH_3PbI_3$ at different average temperatures. Reproduced with permission (Ye et al., 2017). Copyright 2017 the Royal Society of Chemistry.

(D) Seebeck coefficients (S) and (E) the predicted values of the material figure of merit (ZT) as a function of carrier concentration. Reproduced with permission (He and Galli, 2014). Copyright 2014 American Chemical Society

However, the research of HOIPs in this field is still in its primary stage. Singh et al. found that superlattices had an impact on thermoelectric properties. They study the electronic transport properties of HOIPs ($MAPbI_3$ and $MASnI_3$) and their superlattices by using the first-principles computations, material synthesis, and experimental measurements (Singh et al., 2017).

As shown in Figure 10A, five different models are proposed to illustrate the framework of the study. According to the Boltzmann transport theory, the Seebeck coefficient (S), electron contribution to thermal conductivity (k_e), and electrical conductivity per unit relaxation time (σ/τ) could be defined from their calculations.

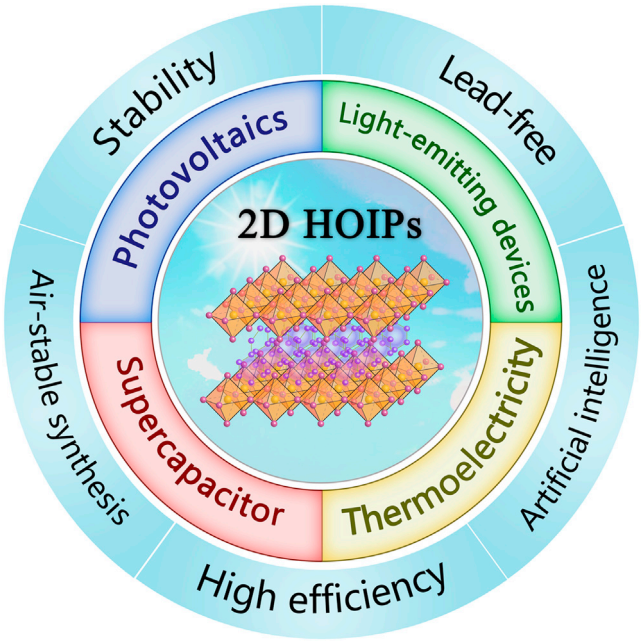

Figure 11. Summary of 2D hybrid organic-inorganic halide perovskites (2D HOIPs) for energy conversion

Compared to superlattices, the calculated values of S, k_e, and σ/τ are smaller, which can be understood because of the fact that the superlattice structures have less average energy than the simple perovskite lattices. According to Filippetti's calculations and the ultralow lattice thermal transport measured recently (Filippetti et al., 2016), HOIPs appeared to become excellent materials for low-cost thermoelectric and solar-thermoelectric applications. For $MAPI_3$, its power factor (σS^2) is about 0.8×10^{-3} W/mK^2, which is not comparable to tellurides and skutterudites (five or six times larger value than the former case) (Filippetti et al., 2016).

However, the relatively small thermal conductivity (k) renders $MAPI_3$ potentially promising thermoelectric (Figure 10B). Ye and coworkers obtained a centimeter-sized of HOIPs $CH_3NH_3PbI_3$ using an improved method of rapid growth (Filippetti et al., 2016). They studied the thermoelectric properties of the $MAPbI_3$ single crystal. They found that the See-beck coefficient of 920 ± 91 mV K^{-1} basically remained unchanged from room temperature to 330 K, and it progressively increased and reached the value of 1693 ± 146 mV K^{-1} at 351 K as shown in Figure 10C.

In contrast, the thermal conductivities have no tendency to be observed as a function of temperature. The thermal conductivities remain between 0.30 and 0.42 W m K^{-1} from 0 to 127°C. To unravel the role of different metal at the B-site in 2D HOIPs on thermoelectric properties, He et al. performed ab-initio calculations to explore thermal transport characteristics of $CH_3NH_3PbI_3$ and $CH_3NH_3SnI_3$ perovskites through the kane single band model (He and Galli, 2014). The figure of merit (ZT) of Pb-based perovskites was greater than that of Sn-perovskite. In addition, the ZT of p-type perovskites was smaller than that of n-type for both perovskites. When the carrier concentration was ca. 10^{18} cm^{-3}, the Seebeck coefficient was large (Figure 10D) and the value of ZT was in the range of one and 2 (Figure 10E). These results indicated that $CH_3NH_3PbI_3$ and $CH_3NH_3SnI_3$ are not only useful in the photovoltaic applications, but in the solar thermoelectric fields.

Mettan's group attempted to increase the ZT of the 2D HOIPs by employing the photo-induced doping (M = Pb) and chemical doping (M = Sn) (Mettan et al., 2015). It turns out that the ZT of $CH_3NH_3SnI_3$ is more than three orders of magnitude higher than the pristine case at room temperature. Temperature-dependent thermal conductivity of $CH_3NH_3PbI_3$ and $CsPbI_3$ is investigated in the range of 7 and 300 K and compare them to the Debye model via the Callaway method. Kovalsky et al. discovered extremely low thermal conductivity of these two materials over the entire temperature range. Moreover, the

$CH_3NH_3PbI_3$ thermal conductivity was lower than that of $CsPbI_3$ (Kovalsky et al., 2017). Extended fitting analyses showed a resonant phonon scattering term (where the frequency associated is in the range of ~15-30 cm^{-1}) linking to the rotational degree of freedom of the organic ion. Therefore, this feature is a responsible factor that suppresses the thermal conductivity of $CH_3NH_3PbI_3$ compared with $CsPbI_3$.

Summary and future prospects

In summary, as 2D HOIPs, have a good foundation for the study of future energy applications, and have been extended to detectors, lasers, transistors, and other technical fields. This review describes the structural, electronic properties, and typical energy applications of 2D HOIPs. Figure 11 depicts the summary of 2D HOIPs for the energy realm. Although 2D HOIPs have good performance and application, the current research is still in its infancy, and there are still many difficulties to be overcome to realize high-performance 2D HOIPs devices. To better use these 2D HOIPs devices in the near future, there are some scientific questions that need to be solved systematically.

(1) Stability of 2D HOIPs. Compared to their bulk phase, the stability of 2D HOIPs is relatively better. However, the most challenging part is the long-term stability, which must be resolved before putting it into the application in energy conversion. There are some ways to extend the long lifetime. First, modifying the material itself, such as doping in A or X to improve entropy contents to form a much more stable phase; Second, modifying the interface, such as increase different bonding to form a stable interfacial layer which can resist moisture, oxygen or UV; Third, modifying the distance, such as using carbon electrode to reduce the penetration into the perovskite layer. Apart from that, heterostructuring of 2D HOIPs would be essential to not only improve the stability, but also enhance physicochemical properties of the hybrid nanocomposites (Shi et al., 2020). Hence, this would be the future direction in 2D HOIPs energy applications.

(2) Artificial intelligence for designing novel 2D HOIPs. In the research field of HOIPs, with the continuous advancement of experimental investigations, data mining effort by using artificial intelligence such as machine learning has also made substantial achievements in recent years (Im et al., 2019; Kirman et al., 2020; Lu et al., 2019). Lu et al. (2018) employed machine learning models from 212 reported HOIPs' band gap values, and then successfully screened six different types of lead-free HOIPs with appropriate electronic band gap and room temperature thermal stability from 5158 untapped potential HOIPs, two of which exhibited direct band gap and excellent environmental stability in the visible light region. Several reasonable prospects are formulated to boost up the progress of 2D HOIPs materials.

The machine learning that assists the compelling design of 2D HOIPs structures is an imperative mainstream trend for the past three years. The state-of-the-art computing technologies envisage important applications to achieve high-throughput screening represented by machine learning in the exploration of newly designed 2D HOIPs structures. At the same time, the development of the Internet of Things (IoT) has promoted the integration of material design and theoretical research. The Internet of things can connect and exchange data with other devices and systems over the Internet, which will be an opportunity for the development of mechanical learning. Combined with first-principles calculations, one can foresee that the large set of 2D HOIPs new materials with highly efficient performance can be constructed using the "bottom-up" approach in the upcoming years.

(3) Novel synthetic approaches for air-stable 2D HOIPs. The existing preparation methods such as spin coating and CVD methods are impractical for large-scale manufacturing processes. It is even more difficult to avoid the problem arising from excessive structural defects when translating the lab-scale to industrial readiness. For this, inspiration can be found from the large-scale manufacture of other emerging 2D materials, such as the stripping and dispersion of bulk materials, taking the perspective of interface and surface effects into consideration.

(4) Lead-free 2D HOIPs. Lead-free development has been gaining in momentum recently to seek a new candidate of hybrid material. Although the current efficiency of lead-free 2D HOIPs is relatively low, researchers have gained a deep understanding of the charge transfer mechanism in these materials through various theoretical methods such as first-principles calculations. This facilitates the construction of highly efficient materials by surface modification and forming heterojunctions with other materials.

(5) Structure-property relationship on the 2D HOIPs system is fundamental toward the rational design and tunable manipulation of their energy-related application. There is an urgent need for systematic research to reveal the correlation between device performance and material properties such as the chemical composition, surface morphology, and crystallinity of 2D HOIPs. Considering that there are a large number of possible combinations between metal cations and organic functional groups within the hybrid materials, using high-throughput screening and synthesis to accelerate the development of new materials in the family of 2D HOIPs. This could trigger efficient solutions to the current challenges in the community of halide perovskite research.

Limitations of the study

Although the current articles on 2D HOIPs are increasing year by year, there are still some unsolved problems such as: (1) the problem of long-term stability must be solved before applying it to energy conversion, (2) the commonly used preparation methods cannot meet the requirements of industrial production At the same time, it is difficult to avoid problems caused by excessive structural defects in industrial production. (3) The efficiency of lead-free 2D HOIPs is relatively low, and there is still a lot of room for development. These issues are major challenges in the development of 2D HOIPs waiting to be crossed by researchers.

ACKNOWLEDGMENTS

N. Li thanks the Natural Science Fund for Distinguished Young Scholars of Hubei Province (No. 2020CFA087); the Overseas Expertise Introduction Project for Discipline Innovation of China (No. B18038); the Basic Research Program of Shenzhen (No. JCYJ20190809120015163), the Central Government Guided Local Science and Technology Development Special Fund Project (2021Szvup106), and Fundamental Research Funds for the Central Universities (2022WUT). J. Jiang thanks for being financially supported by the National Natural Science Foundation of China (No. 62004143); the Central Government Guided Local Science and Technology Development Special Fund Project (No. 2020ZYYD033).

AUTHOR CONTRIBUTIONS

N.L., Z.L. andW.-J.O., took this idea; Y.Y., Z.S., and N.L. surveyed literarure and wrote the manuscript. A.A. and P.Z. carried parts of the writing. N.L., Y.Y., Z.S., Z.L., J.J., and J.L. designed and redrew the figures. All authros discussed the results.

DECLARATION OF INTERESTS

There are no conflicts of interest to declare.

REFERENCES

Abid, H., Hlil, E.K., and Abid, Y. (2017). Spectroscopic ellipsometry thin film and first-principles calculations of electronic and linear optical properties of $[(C_9H_{19}NH_3)_2PbI_2Br_2]$ 2D perovskite. J. Solid State Chem. *247*, 131–136.

Bai, Y., Xiao, S., Hu, C., Zhang, T., Meng, X., Lin, H., Yang, Y., and Yang, S. (2017). Dimensional engineering of a graded 3D–2D halide perovskite interface enables ultrahigh voc enhanced stability in the p-i-n photovoltaics. Adv. Energy Mater. *7*, 1701038.

Beilsten-Edmands, J., Eperon, G.E., Johnson, R.D., Snaith, H.J., and Radaelli, P.G. (2015). Non-ferroelectric nature of the conductance hysteresis in $CH_3NH_3PbI_3$ perovskite-based photovoltaic devices. Appl. Phys. Lett. *106*, 173502..

Blancon, J.-C., Even, J., Stoumpos, C.C., Kanatzidis, M.G., and Mohite, A.D. (2020). Semiconductor physics of organic–inorganic 2D halide perovskites. Nat. Nanotechnol. *15*, 969–985.

Brandt, R.E., Poindexter, J.R., Gorai, P., Kurchin, R.C., Hoye, R.L.Z., Nienhaus, L., Wilson, M.W.B., Polizzotti, J.A., Sereika, R., Žaltauskas, R., et al. (2017). Searching for "defect-tolerant" photovoltaic materials: combined theoretical and experimental screening. Chem. Mater. *29*, 4667–4674.

Bu, T., Li, J., Lin, Q., McMeekin, D.P., Sun, J., Wang, M., Chen, W., Wen, X., Mao, W., McNeill, C.R., et al. (2020). Structure engineering of hierarchical layered perovskite interface for efficient and stable wide bandgap photovoltaics. Nano Energy *75*, 104917.

Byun, J., Cho, H., Wolf, C., Jang, M., Sadhanala, A., Friend, R.H., Yang, H., and Lee, T.-W. (2016). Perovskite light-emitting diodes: efficient visible quasi-2D perovskite light-emitting diodes. Adv. Mater. *28*, 7550.

Chen, W., Wu, Y., Yue, Y., Liu, J., Zhang, W., Yang, X., Chen, H., Bi, E., Ashraful, I., Grätzel, M., et al. (2015). Efficient and stable large-area perovskite solar cells with inorganic charge extraction layers. Science *350*, 944.

Chen, P., Li, N., Chen, X., Ong, W.-J., and Zhao, X. (2017a). The rising star of 2D black phosphorus beyond graphene: synthesis, properties and electronic applications. 2d Mater. *5*, 014002.

Chen, J., Wang, Y., Gan, L., He, Y., Li, H., and Zhai, T. (2017b). Generalized self-doping engineering towards ultrathin and large-sized two-dimensional homologous perovskites. Angew. Chem. Int. Ed. *56*, 14893–14897.

Chen, A.Z., Shiu, M., Ma, J.H., Alpert, M.R., Zhang, D., Foley, B.J., Smilgies, D.-M., Lee, S.-H., and Choi, J.J. (2018). Origin of vertical orientation in two-dimensional metal halide perovskites and its effect on photovoltaic performance. Nat. Commun. *9*, 1336.

Chen, Z., Turedi, B., Alsalloum, A.Y., Yang, C., Zheng, X., Gereige, I., AlSaggaf, A., Mohammed, O.F., and Bakr, O.M. (2019a). Single-crystal $MAPbI_3$ perovskite solar cells exceeding 21% power conversion efficiency. ACS Energy Lett *4*, 1258–1259.

Chen, M., Ju, M.-G., Hu, M., Dai, Z., Hu, Y., Rong, Y., Han, H., Zeng, X.C., Zhou, Y., and Padture, N.P. (2019b). Lead-free dion–jacobson tin halide perovskites for photovoltaics. ACS Energy Lett *4*, 276–277.

Chen, P., Ong, W.-J., Shi, Z., Zhao, X., and Li, N. (2020). Pb-based halide perovskites: recent

advances in photo(electro)catalytic applications and looking beyond. Adv. Funct. Mater. *30*, 1909667.

Choi, J., Le, Q.V., Hong, K., Moon, C.W., Han, J.S., Kwon, K.C., Cha, P.-R., Kwon, Y., Kim, S.Y., and Jang, H.W. (2017). Enhanced endurance organolead halide perovskite resistive switching memories operable under an extremely low bending radius. ACS Appl. Mater. Inter. *9*, 30764–30771.

Dou, L., Wong, A.B., Yu, Y., Lai, M., Kornienko, N., Eaton, S.W., Fu, A., Bischak, C.G., Ma, J., Ding, T., et al. (2015). Atomically thin two-dimensional organic-inorganic hybrid perovskites. Science *349*, 1518.

Du, M.-H., and Singh, D.J. (2010). Enhanced Born charge and proximity to ferroelectricity in thallium halides. Phys. Rev. B *81*, 144114.

Du, M.H. (2014). Efficient carrier transport in halide perovskites: theoretical perspectives. J. Mater. Chem. A. *2*, 9091–9098.

Even, J., Pedesseau, L., Jancu, J.-M., and Katan, C. (2013). Importance of spin–orbit coupling in hybrid organic/inorganic perovskites for photovoltaic applications. J. Phys. Chem. Lett. *4*, 2999–3005.

Fang, Y., Zhang, L., Wu, L., Yan, J., Lin, Y., Wang, K., Mao, W.L., and Zou, B. (2019). Pressure-induced emission (PIE) and phase transition of a two-dimensional halide double perovskite $(BA)_4AgBiBr_8$ ($BA=CH_3(CH_2)_3NH_3^+$). Angew. Chem. Int. Ed. *58*, 15249–15253.

Filippetti, A., Caddeo, C., Delugas, P., and Mattoni, A. (2016). Appealing perspectives of hybrid lead–iodide perovskites as thermoelectric materials. J. Phys. Chem. C *120*, 28472–28479.

Guo, N., Zhang, T., Li, G., Xu, F., Qian, X., and Zhao, Y. (2017a). A simple fabrication of $CH_3NH_3PbI_3$ perovskite for solar cells using low-purity PbI_2. J. Semicond. *38*, 014004.

Guo, Y., Saidi, W.A., and Wang, Q. (2017b). 2D halide perovskite-based van der Waals heterostructures: contact evaluation and performance modulation. 2d Mater. *4*, 035009.

Guo, Y., Yin, X., Liu, J., Chen, W., Wen, S., Que, M., Xie, H., Yang, Y., Que, W., and Gao, B. (2019). Vacuum thermal-evaporated SnO_2 as uniform electron transport layer and novel management of perovskite intermediates for efficient and stable planar perovskite solar cells. Org. Electron. *65*, 207–214.

Ha, S.T., Liu, X., Zhang, Q., Giovanni, D., Sum, T.C., and Xiong, Q. (2014). Synthesis of organic–inorganic lead halide perovskite nanoplatelets: towards high-performance perovskite solar cells and optoelectronic devices. Adv. Opt. Mater. *2*, 838–844.

Ha, S.-T., Shen, C., Zhang, J., and Xiong, Q. (2016). Laser cooling of organic–inorganic lead halide perovskites. Nat. Photon. *10*, 115–121.

He, Y., and Galli, G. (2014). Perovskites for solar thermoelectric applications: a first principle study of $CH_3NH_3AI_3$ (A = Pb and Sn). Chem. Mater. *26*, 5394–5400.

Herz, L.M. (2017). Charge-carrier mobilities in metal halide perovskites: fundamental mechanisms and limits. ACS Energy Lett *2*, 1539–1548.

Hu, X., Zhou, H., Jiang, Z., Wang, X., Yuan, S., Lan, J., Fu, Y., Zhang, X., Zheng, W., and Wang, X. (2017). Direct vapor growth of perovskite $CsPbBr_3$ nanoplate electroluminescence devices. ACS nano *11*, 9869–9876.

Huang, C., Gao, Y., Wang, S., Zhang, C., Yi, N., Xiao, S., and Song, Q. (2017). Giant blueshifts of excitonic resonances in two-dimensional lead halide perovskite. Nano Energy *41*, 320–326.

Huang, Y., Li, Y., Lim, E.L., Kong, T., Zhang, Y., Song, J., Hagfeldt, A., and Bi, D. (2021). Stable layered 2D perovskite solar cells with an efficiency of over 19% via multifunctional interfacial engineering. J. Am. Chem. Soc. *143*, 3911–3917.

Im, J., Lee, S., Ko, T.-W., Kim, H.W., Hyon, Y., and Chang, H. (2019). Identifying Pb-free perovskites for solar cells by machine learning. NPJ Comput. Mater. *5*, 37.

Ishihara, T., Takahashi, J., and Goto, T. (1989). Exciton state in two-dimensional perovskite semiconductor $(C_{10}H_{21}NH_3)_2PbI_4$. Solid State Commun. *69*, 933–936.

Iyikanat, F., Sari, E., and Sahin, H. (2017). Thinning $CsPb_2Br_5$ perovskite down to monolayers: Cs-dependent stability. Phys. Rev. B *96*, 155442.

Jeon, N.J., Noh, J.H., Kim, Y.C., Yang, W.S., Ryu, S., and Seok, S.I. (2014). Solvent engineering for high-performance inorganic–organic hybrid perovskite solar cells. Nat. Mater. *13*, 897–903.

Jeon, N.J., Noh, J.H., Yang, W.S., Kim, Y.C., Ryu, S., Seo, J., and Seok, S.I. (2015). Compositional engineering of perovskite materials for high-performance solar cells. Nature *517*, 476–480.

Jeong, J., Kim, M., Seo, J., Lu, H., Ahlawat, P., Mishra, A., Yang, Y., Hope, M.A., Eickemeyer, F.T., Kim, M., et al. (2021). Pseudo-halide anion engineering for α-$FAPbI_3$ perovskite solar cells. Nature *592*, 381–385.

Jiang, J., Wong, C.P.Y., Zou, J., Li, S., Wang, Q., Chen, J., Qi, D., Wang, H., Eda, G., Chua, D.H.C., et al. (2017). Two-step fabrication of single-layer rectangular SnSe flakes. 2d Mater. *4*, 021026.

Jiang, J., Li, N., Zou, J., Zhou, X., Eda, G., Zhang, Q., Zhang, H., Li, L.-J., Zhai, T., and Wee, A.T.S. (2019). Synergistic additive-mediated CVD growth and chemical modification of 2D Mater. Chem. Soc. Rev. *48*, 4639–4654.

Jo, Y., Oh, K.S., Kim, M., Kim, K.-H., Lee, H., Lee, C.-W., and Kim, D.S. (2016). High performance of planar perovskite solar cells produced from PbI_2(DMSO) and PbI_2(NMP) complexes by intramolecular exchange. Adv. Mater. Inter. *3*, 1500768.

Kagan, C.R., Mitzi, D.B., and Dimitrakopoulos, C.D. (1999). Organic-inorganic hybrid materials as semiconducting channels in thin-film field-effect transistors. Science *286*, 945.

Kataoka, T., Kondo, T., Ito, R., Sasaki, S., Uchida, K., and Miura, N. (1993). Magneto-optical study on excitonic spectra in $(C_6H_{13}NH_3)_2PbI_4$. Phys. Rev. B Condens. Matter *47*, 2010–2018.

Kim, B.-S., Kim, T.-M., Choi, M.-S., Shim, H.-S., and Kim, J.-J. (2015). Fully vacuum–processed perovskite solar cells with high open circuit voltage using MoO_3/NPB as hole extraction layers. Org. Electron. *17*, 102–106.

Kim, H., Han, J.S., Choi, J., Kim, S.Y., and Jang, H.W. (2018). Halide perovskites for applications beyond photovoltaics. Small Methods *2*, 1700310.

Kim, H., Han, J.S., Kim, S.G., Kim, S.Y., and Jang, H.W. (2019a). Halide perovskites for resistive random-access memories. J. Mater. Chem. C *7*, 5226–5234.

Kim, Y.-H., Kim, J.S., and Lee, T.-W. (2019b). Strategies to improve luminescence efficiency of metal-halide perovskites and light-emitting diodes. Adv.Mater. *31*, 1804595.

Kim, H., Huynh, K.A., Kim, S.Y., Le, Q.V., and Jang, H.W. (2020a). 2D and quasi-2D halide perovskites: applications and progress. Phys. Status Solidi R. *14*, 1900435.

Kim, H., Choi, M.-J., Suh, J.M., Han, J.S., Kim, S.G., Le, Q.V., Kim, S.Y., and Jang, H.W. (2020b). Quasi-2D halide perovskites for resistive switching devices with ON/OFF ratios above 109. NPG Asia Mater. *12*, 21.

Kirman, J., Johnston, A., Kuntz, D.A., Askerka, M., Gao, Y., Todorović, P., Ma, D., Privé, G.G., and Sargent, E.H. (2020). Machine-learning-accelerated perovskite crystallization. Matter *2*, 938–947.

Koh, T.M., Shanmugam, V., Schlipf, J., Oesinghaus, L., Müller-Buschbaum, P., Ramakrishnan, N., Swamy, V., Mathews, N., Boix, P.P., and Mhaisalkar, S.G. (2016). Nanostructuring mixed-dimensional perovskites: a route toward tunable, efficient photovoltaics. Adv.Mater. *28*, 3653–3661.

Kojima, A., Teshima, K., Shirai, Y., and Miyasaka, T. (2009). Organometal halide perovskites as visible-light sensitizers for photovoltaic cells. J. Am. Chem. Soc. *131*, 6050–6051.

Kovalsky, A., Wang, L., Marek, G.T., Burda, C., and Dyck, J.S. (2017). Thermal conductivity of $CH_3NH_3PbI_3$ and $CsPbI_3$: measuring the effect of the methylammonium ion on phonon scattering. J. Phys. Chem. C *121*, 3228–3233.

Lang, F., Gluba, M.A., Albrecht, S., Rappich, J., Korte, L., Rech, B., and Nickel, N.H. (2015). Perovskite solar cells with large-area CVD-graphene for tandem solar cells. J. Phys. Chem. Lett. *6*, 2745–2750.

Lee, M.M., Teuscher, J., Miyasaka, T., Murakami, T.N., and Snaith, H.J. (2012). Efficient hybrid solar cells based on meso-superstructured organometal halide perovskites. Science *338*, 643–647.

Lermer, C., Birkhold, S.T., Moudrakovski, I.L., Mayer, P., Schoop, L.M., Schmidt-Mende, L., and Lotsch, B.V. (2016). Toward fluorinated spacers for MAPI-derived hybrid perovskites: synthesis, characterization, and phase transitions of $(FC_2H_4NH_3)_2PbCl_4$. Chem. Mater. *28*, 6560–6566.

Lewis, D.J., and O'Brien, P. (2014). Ambient pressure aerosol-assisted chemical vapour deposition of $(CH_3NH_3)PbBr_3$, an inorganic–

organic perovskite important in photovoltaics. Chem. Commun. *50*, 6319–6321.

Leyden, M.R., Ono, L.K., Raga, S.R., Kato, Y., Wang, S., and Qi, Y. (2014). High performance perovskite solar cells by hybrid chemical vapor deposition. J. Mater. Chem. A. *2*, 18742–18745.

Li, N., Zhu, Z., Chueh, C.-C., Liu, H., Peng, B., Petrone, A., Li, X., Wang, L., and Jen, A.K.Y. (2017). Mixed cation $FA_xPEA_{1-x}PbI_3$ with enhanced phase and ambient stability toward high-performance perovskite solar cells. Adv. Energy Mater. *7*, 1601307.

Li, N., Peng, J., Ong, W.-J., Ma, T., Arramel, Zhang, P., Jiang, J., Yuan, X., and Zhang, C. (2021). MXenes: an emerging platform for wearable electronics and looking beyond. Matter *4*, 377–407.

Lin, Y., Bai, Y., Fang, Y., Chen, Z., Yang, S., Zheng, X., Tang, S., Liu, Y., Zhao, J., and Huang, J. (2018). Enhanced thermal stability in perovskite solar cells by assembling 2D/3D stacking structures. J. Phys. Chem. Lett. *9*, 654–658.

Lin, C.-H., Cheng, B., Li, T.-Y., Retamal, J.R.D., Wei, T.-C., Fu, H.-C., Fang, X., and He, J.-H. (2019). Orthogonal lithography for halide perovskite optoelectronic nanodevices. ACS Nano *13*, 1168–1176.

Liu, M., Johnston, M.B., and Snaith, H.J. (2013). Efficient planar heterojunction perovskite solar cells by vapour deposition. Nature *501*, 395–398.

Liu, X., Niu, L., Wu, C., Cong, C., Wang, H., Zeng, Q., He, H., Fu, Q., Fu, W., and Yu, T. (2016). Periodic organic–inorganic halide perovskite microplatelet arrays on silicon substrates for room-temperature lasing. Adv. Sci. *3*, 1600137.

Liu, J., Leng, J., Wu, K., Zhang, J., and Jin, S. (2017a). Observation of internal photoinduced electron and hole separation in hybrid two-dimentional perovskite films. J. Am. Chem. Soc. *139*, 1432–1435.

Liu, L., Huang, S., Pan, L., Shi, L.-J., Zou, B., Deng, L., and Zhong, H. (2017b). Colloidal synthesis of $CH_3NH_3PbBr_3$ nanoplatelets with polarized emission through self-organization. Angew. Chem. Int. Ed. *56*, 1780–1783.

Lu, S., Zhou, Q., Ouyang, Y., Guo, Y., Li, Q., and Wang, J. (2018). Accelerated discovery of stable lead-free hybrid organic-inorganic perovskites via machine learning. Nat. Commun. *9*, 3405.

Lu, S., Zhou, Q., Ma, L., Guo, Y., and Wang, J. (2019). Rapid discovery of ferroelectric photovoltaic perovskites and material descriptors via machine learning. Small Methods *3*, 1900360.

Ma, L., Dai, J., and Zeng, X.C. (2017). Two-dimensional single-layer organic–inorganic hybrid perovskite semiconductors. Adv. Energy Mater. *7*, 1601731.

Mao, L., Wu, Y., Stoumpos, C.C., Traore, B., Katan, C., Even, J., Wasielewski, M.R., and Kanatzidis, M.G. (2017a). Tunable white-light emission in single-cation-templated three-layered 2D perovskites $(CH_3CH_2NH_3)_4Pb_3Br_{10-x}Cl_x$. J. Am. Chem. Soc. *139*, 11956–11963.

Mao, L., Wu, Y., Stoumpos, C.C., Wasielewski, M.R., and Kanatzidis, M.G. (2017b). White-light emission and structural distortion in new corrugated two-dimensional lead bromide perovskites. J. Am. Chem. Soc. *139*, 5210–5215.

Mao, L., Ke, W., Pedesseau, L., Wu, Y., Katan, C., Even, J., Wasielewski, M.R., Stoumpos, C.C., and Kanatzidis, M.G. (2018). Hybrid dion–jacobson 2D lead iodide perovskites. J. Am. Chem. Soc. *140*, 3775–3783.

Mao, L., Kennard, R.M., Traore, B., Ke, W., Katan, C., Even, J., Chabinyc, M.L., Stoumpos, C.C., and Kanatzidis, M.G. (2019). Seven-layered 2D hybrid lead iodide perovskites. Chem *5*, 2593–2604.

Mauck, C.M., and Tisdale, W.A. (2019). Excitons in 2D organic–inorganic halide perovskites. Trends Chem. *1*, 380–393.

McMeekin, D.P., Sadoughi, G., Rehman, W., Eperon, G.E., Saliba, M., Hörantner, M.T., Haghighirad, A., Sakai, N., Korte, L., Rech, B., et al. (2016). A mixed-cation lead mixed-halide perovskite absorber for tandem solar cells. Science *351*, 151.

Mehdi, H., Mhamdi, A., and Bouazizi, A. (2020). Effect of perovskite precursor ratios and solvents volume on the efficiency of $MAPbI_{3-x}Cl_x$ mixed halide perovskite solar cells. Mater. Sci. Semicond Process. *109*, 104915.

Mettan, X., Pisoni, R., Matus, P., Pisoni, A., Jaćimović, J., Náfrádi, B., Spina, M., Pavuna, D., Forró, L., and Horváth, E. (2015). Tuning of the thermoelectric figure of merit of $CH_3NH_3MI_3$ (M=Pb,Sn) photovoltaic perovskites. J. Phys. Chem. C *119*, 11506–11510.

Mitzi, D.B., Feild, C.A., Harrison, W.T.A., and Guloy, A.M. (1994). Conducting tin halides with a layered organic-based perovskite structure. Nature *369*, 467–469.

Muljarov, E.A., Tikhodeev, S.G., Gippius, N.A., and Ishihara, T. (1995). Excitons in self-organized semiconductor/insulator superlattices: PbI-based perovskite compounds. Phys. Rev. B *51*, 14370–14378.

Nazarenko, O., Kotyrba, M.R., Wörle, M., Cuervo-Reyes, E., Yakunin, S., and Kovalenko, M.V. (2017). Luminescent and photoconductive layered lead halide perovskite compounds comprising mixtures of cesium and guanidinium cations. Inorg. Chem. *56*, 11552–11564.

Ng, S.-F., Lau, M.Y.L., and Ong, W.-J. (2021). Engineering Layered Double Hydroxide–Based Photocatalysts Toward Artificial Photosynthesis: State-of-the-Art Progress and Prospects (Solar RRL), p. 2000535.

Niu, L., Liu, X., Cong, C., Wu, C., Wu, D., Chang, T.R., Wang, H., Zeng, Q., Zhou, J., Wang, X., et al. (2015). Controlled synthesis of organic/inorganic van der Waals solid for tunable light–matter interactions. Adv. Mater. *27*, 7800–7808.

Niu, L., Zeng, Q., Shi, J., Cong, C., Wu, C., Liu, F., Zhou, J., Fu, W., Fu, Q., and Jin, C. (2016). Controlled growth and reliable thickness-dependent properties of organic–inorganic perovskite platelet crystal. Adv. Funct. Mater. *26*, 5263–5270.

Ong, W.-J., and Shak, K.P.Y. (2020b). 2D/2D heterostructured photocatalysts: an emerging platform for artificial photosynthesis. Solar RRL *4*, 2000132.

Ong, W.-J., Putri, L.K., and Mohamed, A.R. (2020a). Rational design of carbon-based 2D nanostructures for enhanced photocatalytic CO_2 reduction: a dimensionality perspective. Chem. Eur. J. *26*, 9710–9748.

Pandey, M., Jacobsen, K.W., and Thygesen, K.S. (2016). Band gap tuning and defect tolerance of atomically thin two-dimensional organic–inorganic halide perovskites. J. Phys. Chem. Lett. *7*, 4346–4352.

Papadatos, D., Vassilakopoulou, A., and Koutselas, I. (2017). Energy transfer yellow light emitting diodes based on blends of quasi-2D perovskites. J. Lumin. *188*, 567–576.

Park, I.-H., Zhang, Q., Kwon, K.C., Zhu, Z., Yu, W., Leng, K., Giovanni, D., Choi, H.S., Abdelwahab, I., Xu, Q.-H., et al. (2019). Ferroelectricity and rashba effect in a two-dimensional dion-jacobson hybrid organic–inorganic perovskite. J. Am. Chem. Soc. *141*, 15972–15976.

Peng, W., Yin, J., Ho, K.-T., Ouellette, O., De Bastiani, M., Murali, B., El Tall, O., Shen, C., Miao, X., Pan, J., et al. (2017a). Ultralow self-doping in two-dimensional hybrid perovskite single crystals. Nano Lett. *17*, 4759–4767.

Peng, W., Yin, J., Ho, K.-T., Ouellette, O., De Bastiani, M., Murali, B., El Tall, O., Shen, C., Miao, X., Pan, J., et al. (2017b). Ultralow self-doping in two-dimensional hybrid perovskite single crystals. Nano Lett. *17*, 4759–4767.

Peng, J., Chen, X., Ong, W.-J., Zhao, X., and Li, N. (2019). Surface and heterointerface engineering of 2D MXenes and their nanocomposites: insights into electro- and photocatalysis. Chem *5*, 18–50.

Qi, D., Wang, Q., Han, C., Jiang, J., Zheng, Y., Chen, W., Zhang, W., and Wee, A.T.S. (2017). Reducing the Schottky barrier between few-layer $MoTe_2$ and gold. 2d Mater. *4*, 045016.

Ruddlesden, S.N., and Popper, P. (1958). The compound $Sr_3Ti_2O_7$ and its structure. Acta Crystallogr. *11*, 54–55.

Saliba, M., Matsui, T., Domanski, K., Seo, J.-Y., Ummadisingu, A., Zakeeruddin, S.M., Correa-Baena, J.-P., Tress, W.R., Abate, A., Hagfeldt, A., et al. (2016a). Incorporation of rubidium cations into perovskite solar cells improves photovoltaic performance. Science *354*, 206.

Saliba, M., Matsui, T., Seo, J.-Y., Domanski, K., Correa-Baena, J.-P., Nazeeruddin, M.K., Zakeeruddin, S.M., Tress, W., Abate, A., Hagfeldt, A., et al. (2016b). Cesium-containing triple cation perovskite solar cells: improved stability, reproducibility and high efficiency. Energy Environ. Sci. *9*, 1989–1997.

Schmidt, L.C., Pertegás, A., González-Carrero, S., Malinkiewicz, O., Agouram, S., Mínguez Espallargas, G., Bolink, H.J., Galian, R.E., and Pérez-Prieto, J. (2014). Nontemplate synthesis of $CH_3NH_3PbBr_3$ perovskite nanoparticles. J. Am. Chem. Soc. *136*, 850–853.

Shang, Y., Liao, Y., Wei, Q., Wang, Z., Xiang, B., Ke, Y., Liu, W., and Ning, Z. (2019). Highly stable

hybrid perovskite light-emitting diodes based on Dion-Jacobson structure. Sci. Adv. *5*, eaaw8072.

Shao, Y., Yuan, Y., and Huang, J. (2016). Correlation of energy disorder and open-circuit voltage in hybrid perovskite solar cells. Nat. Energy *1*, 15001.

Shao, S., Liu, J., Portale, G., Fang, H.-H., Blake, G.R., ten Brink, G.H., Koster, L.J.A., and Loi, M.A. (2018). Highly reproducible Sn-based hybrid perovskite solar cells with 9% efficiency. Adv. Energy Mater. *8*, 1702019.

Shi, H., and Du, M.-H. (2014). Shallow halogen vacancies in halide optoelectronic materials. Phys. Rev. B *90*, 174103.

Shi, E., Gao, Y., Finkenauer, B.P., Akriti, Coffey, A.H., and Dou, L. (2018). Two-dimensional halide perovskite nanomaterials and heterostructures. Chem. Soc. Rev. *47*, 6046–6072.

Shi, E., Yuan, B., Shiring, S.B., Gao, Y., Akriti, Guo, Y., Su, C., Lai, M., Yang, P., Kong, J., et al. (2020). Two-dimensional halide perovskite lateral epitaxial heterostructures. Nature *580*, 614–620.

Shin, S.S., Yeom, E.J., Yang, W.S., Hur, S., Kim, M.G., Im, J., Seo, J., Noh, J.H., and Seok, S.I. (2017). Colloidally prepared La-doped $BaSnO_3$ electrodes for efficient, photostable perovskite solar cells. Science *356*, 167.

Singh, R., Kottokkaran, R., Dalal, V.L., and Balasubramanian, G. (2017). Engineering band gap and electronic transport in organic–inorganic halide perovskites by superlattices. Nanoscale *9*, 8600–8607.

Smith, I.C., Hoke, E.T., Solis-Ibarra, D., McGehee, M.D., and Karunadasa, H.I. (2014). A layered hybrid perovskite solar-cell absorber with enhanced moisture stability. Angew. Chem. Int. Ed. *53*, 11232–11235.

Srimath Kandada, A.R., Neutzner, S., D'Innocenzo, V., Tassone, F., Gandini, M., Akkerman, Q.A., Prato, M., Manna, L., Petrozza, A., and Lanzani, G. (2016). Nonlinear carrier interactions in lead halide perovskites and the role of defects. J. Am. Chem. Soc. *138*, 13604–13611.

Stoumpos, C.C., Cao, D.H., Clark, D.J., Young, J., Rondinelli, J.M., Jang, J.I., Hupp, J.T., and Kanatzidis, M.G. (2016). Ruddlesden–popper hybrid lead iodide perovskite 2D homologous semiconductors. Chem. Mater. *28*, 2852–2867.

Stoumpos, C.C., Soe, C.M.M., Tsai, H., Nie, W., Blancon, J.-C., Cao, D.H., Liu, F., Traoré, B., Katan, C., Even, J., et al. (2017). High members of the 2D ruddlesden-popper halide perovskites: synthesis, optical properties, and solar cells of $(CH_3(CH_2)_3NH_3)_2(CH_3NH_3)_4Pb_5I_{16}$. Chem *2*, 427–440.

Suleiman, A.A., Huang, P., Jin, B., Jiang, J., Zhang, X., Zhou, X., and Zhai, T. (2020). Space-confined growth of 2D InI showing high sensitivity in photodetection. Adv. Electron. Mater. *6*, 2000284.

Tan, Z., Wu, Y., Hong, H., Yin, J., Zhang, J., Lin, L., Wang, M., Sun, X., Sun, L., Huang, Y., et al. (2016). Two-dimensional $(C_4H_9NH_3)_2PbBr_4$ perovskite crystals for high-performance photodetector. J. Am. Chem. Soc. *138*, 16612–16615.

Tremblay, M.-H., Bacsa, J., Zhao, B., Pulvirenti, F., Barlow, S., and Marder, S.R. (2019). Structures of $(4\text{-Y-}C_6H_4CH_2NH_3)_2PbI_4$ {Y = H, F, Cl, Br, I}: tuning of hybrid organic inorganic perovskite structures from ruddlesden–popper to dion–jacobson limits. Chem. Mater. *31*, 6145–6153.

Tsai, H., Nie, W., Blancon, J.-C., Stoumpos, C.C., Asadpour, R., Harutyunyan, B., Neukirch, A.J., Verduzco, R., Crochet, J.J., Tretiak, S., et al. (2016). High-efficiency two-dimensional Ruddlesden–Popper perovskite solar cells. Nature *536*, 312–316.

Tyagi, P., Arveson, S.M., and Tisdale, W.A. (2015). Colloidal organohalide perovskite nanoplatelets exhibiting quantum confinement. J. Phys. Chem. Lett. *6*, 1911–1916.

Walters, G., Haeberlé, L., Quintero-Bermudez, R., Brodeur, J., Kéna-Cohen, S., and Sargent, E.H. (2020). Directional light emission from layered metal halide perovskite crystals. J. Phys. Chem. Lett. *11*, 3458–3465.

Wang, Y., Zheng, Y., Xu, X., Dubuisson, E., Bao, Q., Lu, J., and Loh, K.P. (2011). Electrochemical delamination of CVD-grown graphene film: toward the recyclable use of copper catalyst. ACS Nano *5*, 9927–9933.

Wang, W., Tadé, M.O., and Shao, Z. (2015a). Research progress of perovskite materials in photocatalysis- and photovoltaics-related energy conversion and environmental treatment. Chem. Soc. Rev. *44*, 5371–5408.

Wang, Y., Shi, Y., Xin, G., Lian, J., and Shi, J. (2015b). Two-dimensional van der Waals epitaxy kinetics in a three-dimensional perovskite halide. Cryst. Growth Des. *15*, 4741–4749.

Wang, N., Cheng, L., Ge, R., Zhang, S., Miao, Y., Zou, W., Yi, C., Sun, Y., Cao, Y., Yang, R., et al. (2016). Perovskite light-emitting diodes based on solution-processed self-organized multiple quantum wells. Nat. Photon. *10*, 699–704.

Wang, Y., Guan, X., Li, D., Cheng, H.-C., Duan, X., Lin, Z., and Duan, X. (2017a). Chemical vapor deposition growth of single-crystalline cesium lead halide microplatelets and heterostructures for optoelectronic applications. Nano Res. *10*, 1223–1233.

Wang, Z., Lin, Q., Chmiel, F.P., Sakai, N., Herz, L.M., and Snaith, H.J. (2017b). Efficient ambient-air-stable solar cells with 2D–3D heterostructured butylammonium-caesium-formamidinium lead halide perovskites. Nat. Energy *2*, 17135.

Wang, Z., Ganose, Alex M., Niu, C., and Scanlon, D.O. (2018). First-principles insights into tin-based two-dimensional hybrid halide perovskites for photovoltaics. J. Mater. Chem. A. *6*, 5652–5660.

Wei, Z., and Xing, J. (2019). The rise of perovskite light-emitting diodes. J. Phys. Chem. Lett. *10*, 3035–3042.

Xiao, Z., Meng, W., Saparov, B., Duan, H.-S., Wang, C., Feng, C., Liao, W., Ke, W., Zhao, D., Wang, J., et al. (2016). Photovoltaic properties of two-dimensional $(CH_3NH_3)_2Pb(SCN)_2I_2$ perovskite: a combined experimental and density functional theory study. J. Phys. Chem. Lett. *7*, 1213–1218.

Xu, C., Wang, L., Liu, Z., Chen, L., Guo, J., Kang, N., Ma, X.-L., Cheng, H.-M., and Ren, W. (2015). Large-area high-quality 2D ultrathin Mo_2C superconducting crystals. Nat. Mater. *14*, 1135–1141.

Xu, Q., Cai, W., Li, W., Sreeprasad, T.S., He, Z., Ong, W.-J., and Li, N. (2018a). Two-dimensional quantum dots: fundamentals, photoluminescence mechanism and their energy and environmental applications. Mater. Today Energy *10*, 222–240.

Xu, J., Liu, J.-B., Wang, J., Liu, B.-X., and Huang, B. (2018b). Prediction of novel p-type transparent conductors in layered double perovskites: a first-principles study. Adv. Funct. Mater. *28*, 1800332.

Yan, L., Hu, J., Zhou, N., Moran, A.M., and You, W. (2020). Enhancing photovoltaic performance of aromatic ammonium-based two-dimensional organic-inorganic hybrid perovskites via tuning $CH\cdots\pi$ interaction. Solar RRL *4*, 1900374.

Yang, W.S., Noh, J.H., Jeon, N.J., Kim, Y.C., Ryu, S., Seo, J., and Seok, S.I. (2015). High-performance photovoltaic perovskite layers fabricated through intramolecular exchange. Science *348*, 1234–1237.

Yao, K., Wang, X., Xu, Y.-x., and Li, F. (2015). A general fabrication procedure for efficient and stable planar perovskite solar cells: morphological and interfacial control by in-situ-generated layered perovskite. Nano Energy *18*, 165–175.

Yao, K., Wang, X., Xu, Y.-x., Li, F., and Zhou, L. (2016). Multilayered perovskite materials based on polymeric-ammonium cations for stable large-area solar cell. Chem. Mater. *28*, 3131–3138.

Ye, T., Wang, X., Li, X., Yan, A.Q., Ramakrishna, S., and Xu, J. (2017). Ultra-high Seebeck coefficient and low thermal conductivity of a centimeter-sized perovskite single crystal acquired by a modified fast growth method. J. Mater. Chem. C *5*, 1255–1260.

Yin, W.-J., Shi, T., and Yan, Y. (2014). Unusual defect physics in $CH_3NH_3PbI_3$ perovskite solar cell absorber. Appl. Phys. Lett. *104*, 063903.

Zejian, W., Jiajia, H., Sue-Faye, N., Wen, L., Junjie, H., Pengfei, C., and Wee-Jun, O. (2021). Recent progress of perovskite oxide in emerging photocatalysis landscape: water splitting, CO_2 reduction, and N_2 fixation. Acta Phys. -Chim. Sin. *37*, 2011033.

Zhang, H., Lin, H., Liang, C., Liu, H., Liang, J., Zhao, Y., Zhang, W., Sun, M., Xiao, W., Li, H., et al. (2015). Organic–inorganic perovskite light-emitting electrochemical cells with a large capacitance. Adv. Funct. Mater. *25*, 7226–7232.

Zhang, Q., Su, R., Liu, X., Xing, J., Sum, T.C., and Xiong, Q. (2016). High-quality whispering-gallery-mode lasing from cesium lead halide perovskite nanoplatelets. Adv. Funct. Mater. *26*, 6238–6245.

Zhang, L., Wu, L., Wang, K., and Zou, B. (2019a). Pressure-induced broadband emission of 2D organic–inorganic hybrid perovskite $(C_6H_5C_2H_4NH_3)_2PbBr_4$. Adv. Sci. *6*, 1801628.

Zhang, X., Jiang, J., Suleiman, A.A., Jin, B., Hu, X., Zhou, X., and Zhai, T. (2019b). Hydrogen-Assisted growth of ultrathin Te flakes with giant gate-dependent photoresponse. Adv. Funct. Mater. *29*, 1906585.

Zhang, W., Mohamed, A.R., and Ong, W.-J. (2020a). Z-scheme photocatalytic systems for carbon dioxide reduction: where are we now? Angew. Chem. Int. Ed. *59*, 22894–22915.

Zhang, F., Lu, H., Tong, J., Berry, J.J., Beard, M.C., and Zhu, K. (2020b). Advances in two-dimensional organic–inorganic hybrid perovskites. Energy Environ. Sci. *13*, 1154–1186.

Zhang, X., Yang, T., Ren, X., Zhang, L., Zhao, K., and Liu, S. (2021). Film formation control for high performance dion–jacobson 2D perovskite solar cells. Adv. Energy Mater. *11*, 2002733.

Zhou, H., Chen, Q., Li, G., Luo, S., Song, T.-b., Duan, H.-S., Hong, Z., You, J., Liu, Y., and Yang, Y. (2014). Interface engineering of highly efficient perovskite solar cells. Science *345*, 542–546.

Zhou, H., Yuan, S., Wang, X., Xu, T., Wang, X., Li, H., Zheng, W., Fan, P., Li, Y., and Sun, L. (2017). Vapor growth and tunable lasing of band gap engineered cesium lead halide perovskite micro/nanorods with triangular cross section. ACS nano *11*, 1189–1195.